IDŐJÁRÁS

QUARTERLY JOURNAL
OF THE HUNGARIAN METEOROLOGICAL SERVICE

CONTENTS

****

http://omsz.met.hu/firat/ido-e.html

VOL. 105 * NO. 3 * JULY–SEPTEMBER 2001

IDŐJÁRÁS

Quarterly Journal of the Hungarian Meteorological Service

Editorial Office: P.O. Box 39, H-1675 Budapest, Hungary or
Gilice tér 39, H-1181 Budapest, Hungary
E-mail: prager.t@met.hu or *antal.e@met.hu*
Fax: (36-1) 346-4809

Subscription by

mail: IDŐJÁRÁS, P.O. Box 39, H-1675 Budapest, Hungary
E-mail: prager.t@met.hu or *antal.e@met.hu*; *Fax: (36-1) 346-4809*

IDŐJÁRÁS

Quarterly Journal of the Hungarian Meteorological Service
Vol. 105, No. 3, July–September 2001, pp. 135–144

Model simulation on the transboundary contribution to the atmospheric sulfur concentration and deposition in Hungary

Ágnes Havasi[1], **László Bozó**[2] and **Zahari Zlatev**[3]

[1]*Department of Meteorology, Eötvös Loránd University,*
P.O. Box 32, H-1518 Budapest, Hungary; E-mail: hagi@nimbus.elte.hu

[2]*Hungarian Meteorological Service,*
P.O. Box 39, H-1675 Budapest, Hungary; E-mail: bozo.l@met.hu

[3]*National Environmental Research Institute of Denmark,*
P.O. Box 358, DK-4000 Roskilde, Denmark; E-mail: zz@dmu.dk

(Manuscript received August 13, 2001; in final form August 30, 2001)

Abstract—Reduction of sulfur emissions in Europe during the past decades have positively contributed to limit exposure to acidification. Based on long-range transport model computations by means of Danish Eulerian Model (DEM) as well as regional background concentration/deposition measurements, the transboundary contribution to the Hungarian sulfur concentration and deposition was estimated for the period of 1989–1998. It was found that despite the intense reduction of sulfur emission in Hungary during the period investigated, Hungary's own sources still significantly contribute to the sulfur deposition in the country. Measured versus modeled sulfur data for Hungary as well as ratios of transboundary and Hungary's own sulfur fluxes are presented and discussed in the paper.

Key-words: transboundary air pollution, Danish Eulerian Model, sulfur deposition.

1. Introduction

European countries of medium or smaller sizes are considerably exposed to the effects of transboundary air pollution. It is caused by the fact that the average atmospheric residence times of several pollutants (e.g., SO_2, sulfate particles) are in the range of a few days that makes possible to transport these species several hundred kilometers far away from their emitting sources. Due to the

deep economic changes during the past decade in the eastern part of Europe, their energy and industry structures were reorganized that resulted in significant decrease of sulfur emission. In the same time, other European countries reduced their sulfur emissions as well. Out-of-date industrial technologies in Hungary are being replaced by less energy consumer and more environment friendly ones. Equipping huge sulfur emitting lignite based thermal power plants with high efficiency sulfur and particle filters is in process at several power plants of Hungary. The rate of annual sulfur emission decreased from 550 kilotonnes (in sulfur) to 300 kilotonnes (S) between 1989 and 1998 (*EMEP,* 2000).

The main goal of present paper is to investigate how the transboundary sulfur flux and its contribution to the Hungarian regional background concentration and deposition rate changed between 1989 and 1998. Computations were based on the two-dimensional version of the European-scale Danish Eulerian Model (DEM) with 50 km × 50 km spatial resolution. Calculations presented in this paper are based on meteorological data obtained by use of EUROLAM, a version of HIRLAM developed at the Norwegian Meteorological Institute in Oslo. (A description of EUROLAM can be found e.g., in *HIRLAM,* 1996.) Regional background air pollution data gained from the EMEP network (including Hungarian monitoring sites) were used for the verification of the model.

2. Description of the Danish Eulerian Model and the model simulations

Part of the results presented in this paper were obtained by using the two-dimensional version of the Danish Eulerian Model. This model has been developed at the National Environmental Research Institute of Denmark for studying the long-range transport of air pollutants over the European region (*Zlatev*, 1995; *Zlatev et al.*, 1994, 1996).

The three-dimensional version of the model is based on the system of q partial differential equations:

$$\frac{\partial c_s}{\partial t} = -\frac{\partial (uc_s)}{\partial x} - \frac{\partial (vc_s)}{\partial y} - \frac{\partial (wc_s)}{\partial z}$$

$$+ \frac{\partial}{\partial x}\left(K_x \frac{\partial c_s}{\partial x} \right) + \frac{\partial}{\partial y}\left(K_y \frac{\partial c_s}{\partial y} \right) + \frac{\partial}{\partial z}\left(K_z \frac{\partial c_s}{\partial z} \right)$$

$$+ E_s - (\kappa_{1s} + \kappa_{2s}) c_s + Q_s(c_1, c_2, ..., c_q), \quad s = 1, ..., q. \qquad (1)$$

Here the unknown concentrations of the chemical species involved in the model are denoted by c_s, u, v and w are the wind velocities, K_x, K_y and K_z are the diffusion coefficients, the source term is denoted by E_s, κ_{1s} and κ_{2s} are the deposition coefficients (for dry and wet deposition, respectively) and the chemical reactions are described by $Q_s(c_1, \ldots, c_q)$. The chemical scheme used at present in the DEM contains $q = 35$ species, so 35 partial differential equations are solved.

It is difficult to treat the system (1) directly. This is the reason why some operator splitting procedure is applied during the numerical solution. A splitting technique, based on ideas proposed in *Marchuk* (1985) and *McRae et al.* (1984) leads, for $s = 1, 2, \ldots, q$, to five sub-models, representing the horizontal advection, the horizontal diffusion, the chemistry (together with the emission terms), the deposition and the vertical transport:

$$\frac{\partial c_s^{(1)}}{\partial t} = -\frac{\partial (u c_s^{(1)})}{\partial x} - \frac{\partial (v c_s^{(1)})}{\partial y},$$

$$\frac{\partial c_s^{(2)}}{\partial t} = \frac{\partial}{\partial x}\left(K_x \frac{\partial c_s^{(2)}}{\partial x} \right) + \frac{\partial}{\partial y}\left(K_y \frac{\partial c_s^{(2)}}{\partial y} \right),$$

$$\frac{\partial c_s^{(3)}}{\partial t} = E_s + Q_s(c_1^{(3)}, c_2^{(3)}, \ldots, c_q^{(3)}),$$

$$\frac{\partial c_s^{(4)}}{\partial t} = -(\kappa_{1s} + \kappa_{2s}) c_s^{(4)},$$

$$\frac{\partial c_s^{(5)}}{\partial t} = -\frac{\partial (w c_s^{(5)})}{\partial z} + \frac{\partial}{\partial z}\left(K_z \frac{\partial c_s^{(5)}}{\partial z} \right). \qquad (2)$$

The discretization of the spatial derivatives in the sub-models leads to the solution (successively at each time-step) of five systems ($i = 1, 2, 3, 4, 5$) of ordinary differential equations:

$$\frac{dg^{(i)}}{dt} = f^{(i)}(t, g^{(i)}), \quad g^{(i)} \in R^{N_x \times N_y \times N_z \times q}, \quad f^{(i)} \in R^{N_x \times N_y \times N_z \times q}, \qquad (3)$$

where N_x, N_y and N_z are the numbers of grid-points along the coordinate axes, the functions $f^{(i)}$, $i = 1, 2, 3, 4, 5$ depend on the particular discretization

methods used in the numerical treatment of the different sub-models, while the functions $g^{(i)}$, $i = 1, 2, 3, 4, 5$ contain approximations of the concentrations at the grid-points of the space domain. (More details about the splitting procedure and about the numerical treatment of the sub-models can be found, among others, in *Alexandrov et al.* (1997), *Hov et al.* (1988) and *Zlatev* (1995)).

The space domain of the model contains whole Europe together with parts of Asia, Africa and the Atlantic Ocean. In the basic version, which is also used in this study, the horizontal plane has been discretized by using a 96 × 96 grid, which means that the number of grid-cells is 9216 and the grid resolution is approximately 50 km × 50 km. (This is a sub-grid of the original 150 km × 150 km resolution EMEP grid.) In the vertical direction the grid is non-equidistant: the increments are smaller close to the surface and become larger towards the top boundary. Ten vertical layers are used at present.

The initial conditions for the system (1) are either available from a previous run of the model or obtained after a five-day start-up period. In the latter case the computations are started five days before the desired starting date with some background concentrations, and the concentrations found at the end of the fifth day are actually used as initial concentrations.

The lateral boundary conditions are represented in the DEM with typical background concentrations varied both diurnally and seasonally. The upper boundary condition is similar to that used in *Simpson* (1992) (see the curves in Fig. 2 in this reference).

The meteorological and emission input data have been prepared within the EMEP (*Vestreng* and *Støren*, 2000) and provided by the Norwegian Meteorological Institute.

The meteorological data contain horizontal wind velocity fields, vertical wind velocity fields (on the top of the boundary layer), precipitation fields, humidity fields, cloud covers, mixing heights and pressures. The resolution of the meteorological fields is coarser than the resolution used in the model: the time resolution for all fields except the mixing height fields is six hours (for the mixing height fields the resolution is 12 hours), while the spatial resolution is approximately 150 km × 150 km. Simple linear interpolation rules are used both in time and space to calculate the grid-point values for the finer grid of the DEM.

Emission of five chemical species are taken into consideration in the DEM: SO_2, NO_2, anthropogenic VOC, ammonia-ammonium and natural VOC emissions. The emission data in the first four fields are annual totals available on a 50 km × 50 km grid. Simple rules are used to get seasonal variations for the SO_2 emissions and the ammonia-ammonium emissions. Both seasonal variations and diurnal variations are simulated for the NO_x emissions and for the anthropogenic VOC emissions.

3. Results of the model computations

DEM model outputs for SO_2 concentrations in 1997 were compared with those of measured at 3 monitoring sites in Hungary. Results are plotted in *Fig. 1.*

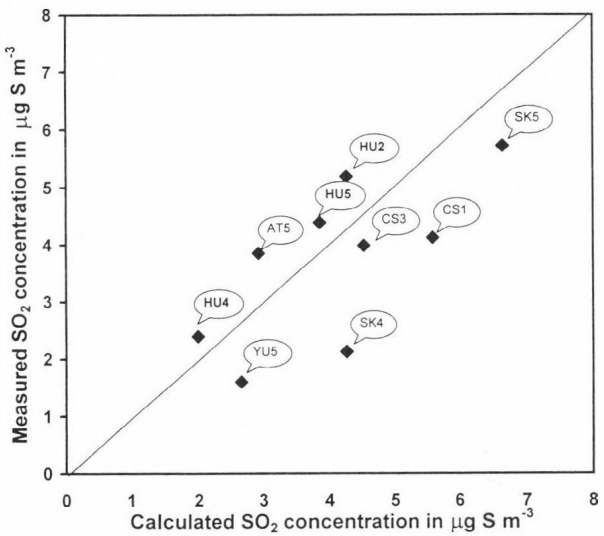

Fig. 1. Measured *vs* computed SO_2 concentrations (annual averages for 1997) at selected monitoring sites in central Europe.

Abbreviations of HU2, HU4 and HU5 represent K-puszta (central part of Hungary), Farkasfa (western part of Hungary) and Hortobágy (eastern part of Hungary), respectively. Results from a few other stations located in the Czech Republic (CS) , Austria (AT) , Slovakia (SK) and Yugoslavia (YU) are also plotted in the figure. It can be seen that model simulations slightly underestimate the annual average concentrations for all three Hungarian stations. The plots are, however, very close to the theoretical fitting line. Regarding the Hungarian monitoring sites, the lowest annual average concentrations in 1997 were simulated and measured for Farkasfa, while the highest ones for K-puszta. There is a factor of 2.2 between the annual average concentrations measured at K-puszta and Farkasfa. There is a four years long (1997–2000) simultaneous SO_2 measurement record from Farkasfa, K-puszta and Hortobágy. Sampling is based on 24 h exposure times at all the three stations. Annual averages are shown in *Fig. 2.* It can be concluded from the figure that each station recorded a decreasing concentration trend: lowest averages were calculated for Farkasfa while the highest ones for K-puszta during the entire

observation period. It can be stated that western part of the country is less exposed to atmospheric SO_2 pollution than central and eastern parts of Hungary.

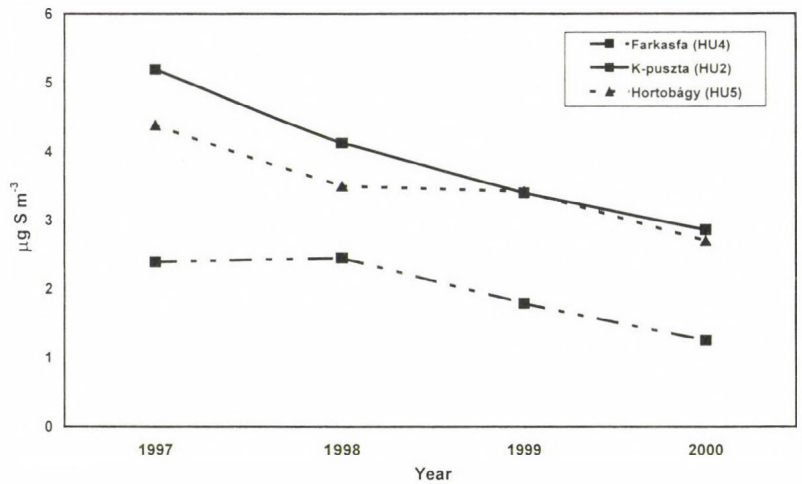

Fig. 2. Annual averages of SO_2 concentrations at three sites in Hungary, 1997–2000.

Model computations were performed with DEM to estimate annual average sulfur-dioxide concentrations in Hungary. Temporal variation of the modeled SO_2 concentration in Hungary during the period of 1989–1998 is shown in *Fig. 3.* Concentration values were averaged for the grids covering Hungary. It was estimated by means of model computations, to which extent the transboundary sources contributed to the sulfur-dioxide concentration over Hungary. Due to the model outputs, the percentage contributions of transboundary sulfur-dioxide emitters varied between 49% (in 1996) and 54% (in 1990 and 1992). Measured annual average sulfur-dioxide concentrations are also indicated in the figure: for the period of 1989–1992 only the data from K-puszta station were available, and between 1993–1995 even this sulfur-dioxide data record is incomplete and can not be used for evaluation. In 1996, however, two additional stations, Farkasfa and Hortobágy joined the regional background air pollution monitoring network in Hungary: the average of their annual sulfur-dioxide concentrations is plotted in the figure for the period of 1996-1998. It should be noted, that despite the continuous decrease in SO_2 emissions in all countries in the region during the second half of the 90's, a local annual maximum was detected in 1997 at all Hungarian stations as well as in the DEM model outputs. It might be explained by the variation of mete-

orological parameters (wind direction, precipitation amount, atmospheric stability, etc.) that requires further investigation in the future.

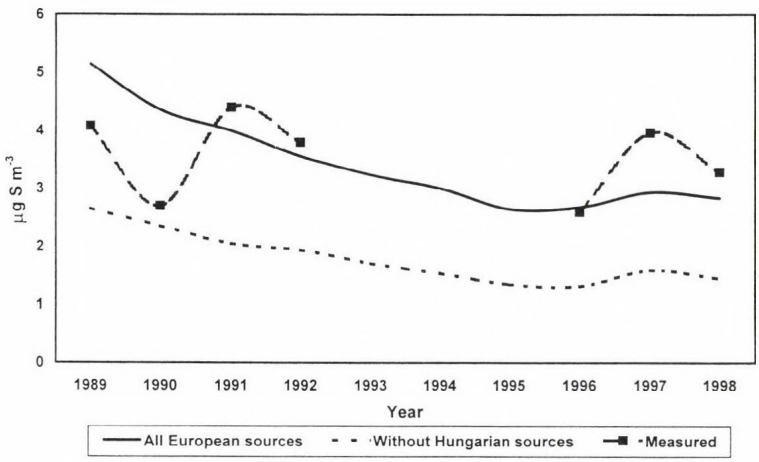

Fig. 3. Results of annual average SO_2 concentration simulations and measurements.

Temporal variations of measured and computed sulfate wet depositions are plotted in *Fig. 4.* Model computations were performed for two different cases:

(1) including all European sulfur sources and

(2) European sources without the input of Hungarian emitters.

It can be concluded from the model calculations that percentage contribution of transboundary sources to the wet sulfur depositions varied between 53% (1996) and 58% (1993) so Hungarian emitters are responsible for wet sulfur deposition at a rate of less than 50%. Wet deposition of sulfur is measured by means of wet only samplers at the regional background air pollution stations. Rate of wet sulfur deposition is calculated by multiplying the sulfate concentration by the amount of precipitation. Results of measurements are also plotted in the figure. It can be seen that rather good agreement between the modeled and observed (K-puszta) values was found for the period of 1993–1998. For the period of 1989–1992, model outputs significantly overestimate the rate of sulfate deposition measured. It should be noted, however, that measurements carried out at K-puszta station might not be representative for the whole country where the outputs of model computations refer to.

Wet deposition of sulfur-dioxide and sulfate can only been measured altogether as the sulfate content of precipitation. Based on DEM parameterization, the rain-out and wash-out processes for sulfur-dioxide and sulfate were separated. *Fig. 5.* shows the rate of wet sulfate deposition and the fraction of sulfate deposited over Hungary originates from sulfur-dioxide. It was estimated that SO_2 contributes at a rate of approximately 80% to the rate of wet sulfate deposition in Hungary.

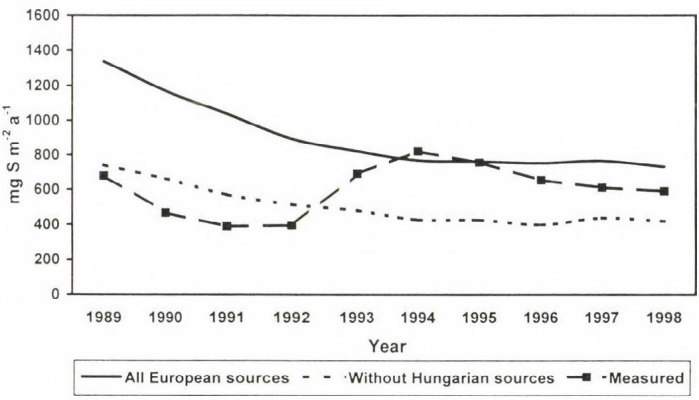

Fig. 4. Results of the simulations and measurements for the rate of wet sulfate deposition.

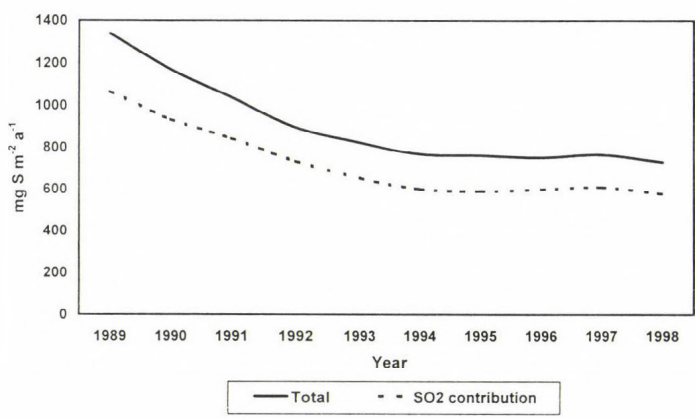

Fig. 5. Plot of SO_2 contribution to the rate of wet sulfate deposition in Hungary, simulated by DEM.

Transboundary contribution to the rate of sulfur deposition in Hungary was compared with the outputs for the same country computed by means of the EMEP Eulerian model (*EMEP,* 2000). Results of comparison is shown in *Fig. 6.*

Based on the EMEP model computations, 4.7 Mtonnes (S) of the 8.0 Mtonnes (S) deposited on EMEP area was originated from the transboundary exchange of pollution among these countries and neighboring areas. Figure also contains data on the percentage contribution of transboundary sources to nitrogen, lead and cadmium deposition: results for nitrogen were reported in *EMEP* (2000), while percentage contributions of lead were taken from *Bozó* (2000), whose computations were performed by means of a European scale Lagrangian-model (TRACE) developed for the investigation of the long-range atmospheric transport and deposition of trace metals. Data for cadmium were obtained from *Ilyin et al.* (2001). It can be concluded from the figure that there is a good agreement between the outputs of DEM and EMEP models for sulfur deposition. Rates of percentage transboundary contributions to lead and cadmium depositions are considerably higher than those of acidifying and eutrophying sulfur and nitrogen compounds.

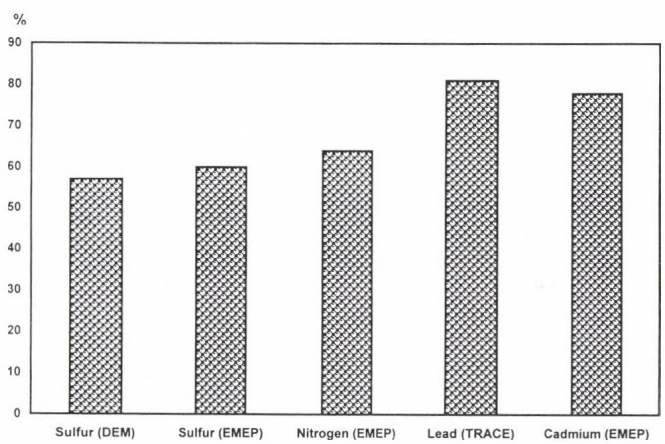

Fig. 6. Percentage contribution of transboundary sources to the total sulfur, nitrogen, lead and cadmium depositions in Hungary.

4. Conclusions

- Model simulations performed by DEM slightly underestimate the annual average concentrations for all the three Hungarian stations. There is little bias in annual averages for 1997.

- Each Hungarian regional background station reported a decreasing concentration trend of sulfur-dioxide between 1997–2000: lowest averages were calculated for Farkasfa (western part of Hungary), while the highest ones

for K-puszta (central part of Hungary) during the entire observation period. It can be stated that western part of the country is less exposed to atmospheric SO_2 pollution than central and eastern parts of Hungary.

- Model outputs show that the percentage contributions of transboundary sulfur-dioxide emitters to the ambient concentration level in Hungary varied between 49% (in 1996) and 54% (computed for 1990 and 1992).
- Percentage contribution of transboundary sources to the rate of wet sulfur depositions in Hungary varied between 53% (1996) and 58% (1993), so Hungarian emitters are responsible for wet sulfur deposition at a rate of less than 50%.
- It was estimated that SO_2 contributes at a rate of approximately 80% to the rate of wet sulfate deposition in Hungary.

Acknowledgements—This paper was partly supported by Hungarian Scientific Research Fund (OTKA T031997).

References

Alexandrov, V., Sameh, A., Siddique, Y. and *Zlatev, Z.*, 1997: Numerical integration of chemical ODE problems arising in air pollution models. *Environmental Modelling and Assessment 2,* 365-377.

Bozó, L., 2000: Estimation of historical atmospheric lead (Pb) deposition over Hungary. *Időjárás 104*, 161-172.

EMEP, 2000: Transboundary Acidification and Eutrophication in Europe. *EMEP Report 1/2000.* Norwegian Meteorological Institute, EMEP CCC and MSC- West.

HIRLAM, 1996: Documentation Manual, *HIRLAM PROJECT,* Research and Development Division, Norwegian Meteorological Institute, PB43, Blindern, 0313 Oslo, Norway.

Hov, Ø., Zlatev, Z., Berkowicz, R., Eliassen, A. and *Prahm, L. P.*, 1988: Comparison of numerical techniques for use in air pollution models with non-linear chemical reactions. *Atmospheric Environment 23,* 967-983.

Ilyin, I., Ryaboshapko, A., Afinogenova, O., Berg, T. and *Hjellbrekke, A.-G.* 2001: Evaluation of transboundary transport of heavy metals in 1999. Trend analysis. EMEP Report 3/2001. EMEP MSC - East.

Marchuk, G. I., 1985: Mathematical modelling for the problem of the environment. *Studies in Mathematics and Applications 16,* North-Holland, Amsterdam.

Simpson, D., 1992: Long-period modelling of photochemical oxidants in Europe. Model calculations for July. *Atmospheric Environment 26A,* 1609.

Vestreng, V. and *Støren, E.*, 2000: Analysis of UNECE/EMEP emission data, MSC-W Status Report 2000. *EMEP MSC-W Note 1/00, July 2000.* Meteorological Synthesizing Centre - West, Norwegian Meteorological Institute, P.O. Box 43 - Blindern, N-0313 Oslo 3, Norway.

Zlatev, Z., Dimov, I. and *Georgiev, K.*, 1994: Studying long-range transport of air pollutants. *Computational Science and Engineering 1*, 45-52.

Zlatev, Z., 1995: *Computer Treatment of Large Air Pollution Models.* Kluwer Academic Publishers.

Zlatev, Z., Dimov, I. and *Georgiev, K.*, 1996: Three-dimensional version of the Danish Eulerian Model. *Zeitschrift für Angewandte Mathematik und Mechanik 76*, 473-476.

IDŐJÁRÁS

Quarterly Journal of the Hungarian Meteorological Service
Vol. 105, No. 3, July–September 2001, pp. 145 –156

Characterization of atmospheric aerosol particles over Lake Balaton, Hungary, using X-ray emission methods

J. Osán[1†], B. Alföldy[1], S. Kurunczi[1], S. Török[1], L. Bozó[2], A. Worobiec[3], J. Injuk[3] and R. Van Grieken[3]

[1]*KFKI Atomic Energy Research Institute, P.O. Box 49, H-1525 Budapest, Hungary*
[2]*Hungarian Meteorological Service, P.O. Box 39, H-1675 Budapest, Hungary*
[3]*Department of Chemistry, University of Antwerp, Universiteitsplein 1, B-2610 Antwerpen, Belgium*

(Manuscript received May 24, 2001; in final form August 6, 2001)

Abstract—Aerosol samples were collected using Berner-type cascade impactor and stacked filter units at Siófok during four campaigns in 1999 and 2000. A total of 40 bulk samples were measured using X-ray fluorescence (XRF). The concentrations of light elements in individual particles were calculated using a reverse Monte Carlo method developed at the University of Antwerp. The particles were further classified using hierarchical and non-hierarchical cluster analyses. Around 25,000 individual particles were analyzed by computer-controlled electron probe microanalysis (EPMA). In order to determine the possible sources of the aerosol particles, the combined data set of the bulk XRF and single-particle EPMA results was subjected to principal component analysis. The obtained analytical results were compared to the air mass backward trajectories, showing good correlation for the sampling periods. The composition of the aerosol did not show characteristic seasonal variation, it was more correlated to the origin of the incoming air mass.

Key-words: aerosol deposition, single particle analysis, light element analysis, X-ray fluorescence.

1. Introduction

Lake Balaton is the largest lake in Central Europe (596 km^2). It has shallow water (average depth is 3 m, maximum depth is 11 m) and hence, because of its relatively low water volume, it is very vulnerable to pollution problems; indeed, dilution of pollutants is limited in Lake Balaton. On its northern part,

† Corresponding author; E-mail: osan@sunserv.kfki.hu

it is surrounded by picturesque hills and small villages. From May to September, many Hungarian tourists, and also millions of foreign visitors take their vacation there. The population around the Lake is several times higher in summer than in winter. A number of Government Decisions were issued during the last decade to improve the water and air quality in the region. They included the cleaning of the Zala river, which empties into Lake Balaton, the building up of the whole sewage water drain system around the Lake, etc. Environmental and human health concerns of atmospheric aerosol pollution in the region are three-fold:

- atmospheric deposition and accumulation of toxic metals and nutrients from urban and industrial emissions into the Lake with possible adverse effects on the ecology;
- air quality (inhalation); and
- visibility (controlled by sulfate particles).

So far, no extended environmental campaigns, with emphasis on the atmospheric heavy metal and nutrient inputs, have been carried out in the Lake region. It is suspected that the atmosphere could be an important source of environmental deterioration of the Lake, relative to the pollutant supply by rivers and direct discharges. Aerosol monitoring took place recently around the Lake, but the analyses included only concentration, fractionation and deposition of non-volatile heavy metals (*Hlavay et al.,* 2001). Only a preliminary paper appeared hitherto on the deposition of nitrogen and phosphorus into Lake Balaton (*Horváth et al.,* 1981). As such, we would like to pay attention to the following target compounds:

(i) particulate nitrogen and phosphorus compounds;

(ii) aluminum, silicon, manganese and iron which have also biological roles; and

(iii) heavy metals, which have been recognized as being toxic, i.e., chromium, nickel, copper, zinc, cadmium and lead.

On a global and regional scale, atmospheric inputs to the ocean environment are known to be an important source of nutrients like nitrogen and bioavailable trace elements, including silicon, manganese, iron, cobalt, nickel, copper and zinc, which play a key role in primary production and influence oceanic productivity. With respect to heavy metals, direct deposition from the atmosphere was recognized about fifteen years ago as a potentially major input for the North Sea (*Van Malderen et al.,* 1992). In this study, the findings for oceanic environments will be compared to the situation over a shallow lake.

Low-Z elemental analysis is mandatory when nutrient elements like nitrogen and phosphorus, have to be determined together with polluting metals. A recently developed method based on thin-window electron probe microanalysis (EPMA) enables the simultaneous determination of major low-Z and minor elements (*Osán et al.,* 2000), even at the single particle level, allowing chemical speciation on a micrometer scale. The full information provided by low-Z EPMA compared with air mass backward trajectories enables the identification of the sources of the particles without the need of combined measurements. In addition, the bulk trace element composition of the aerosol was studied using X-ray fluorescence (XRF) analysis.

2. Experimental

2.1 Samples

Aerosol samples were collected at the Siófok station of the Hungarian Meteorological Service during four campaigns in July 1999, February, June and September 2000. The meteorological station is located at the lakeshore, and can only be reached through a dead-end street with local traffic. The samplers were placed in the grassy backyard, at 2 m height, and around 10 m from the lake. A total of 29 TSP samples were taken on 0.4 μm pore-size Nuclepore filters, for bulk trace element analysis. 24-hour samples were collected daily during the campaigns. Stacked filter units were used for collection of coarse (2.5–10 μm) and fine (<2.5 μm) aerosol particles, for scanning electron microscope (SEM) visualization and single particle analysis. The coarse particles were collected on a 8.0 μm pore size Nuclepore filter, while the fine fraction was obtained on a 0.4 μm pore size Nuclepore filter. A total of 19 sets of size-fractionated samples were collected using a nine-stage Berner-type cascade impactor, on Al, Ag and Be foils as well as Si wafers. The aerodynamic cut-off diameters are 0.0625, 0.125, 0.25, 0.5, 1, 2, 4, 8 and 16 μm, for stages 1–9, respectively. The sampling time varied between 1 (for stage 3) and 240 (for stage 8) minutes, to obtain the best loading of particles in the impacted spots. Around 25,000 individual particles collected on stages 3–7 were analyzed using thin-window EPMA.

2.2 Methods

The bulk trace element analysis of the aerosol loaded Nuclepore filters was performed by an automated Tracor Spectrace 5000 EDXRF system (Tracor X-ray, CA, U.S.A.) coupled with a PC that controls the spectrometer and the

data acquisition. The Spectrace-5000 uses a lower power Rh-anode X-ray tube (17.5 W). In our measurements, the whole white spectrum generated by the tube was used for excitation of the samples under vacuum conditions. Emergent X-rays were detected at 90° relative to the incident X-ray beam by a Si(Li) detector. A standard operating procedure for the XRF analysis of aerosols on filters has been followed according to the guidelines of U.S. Environmental Protection Agency (US EPA). In the calibration procedure, a series of thin film reference standards (Micromatter, Seattle, WA, U.S.A.) were used. The acquired X-ray spectra were deconvoluted with a non-linear least-squares fitting procedure, using the AXIL software (*Vekemans et al.*, 1994). For quantitative analysis of the samples, the fundamental parameter method proposed by *Szalóki* (1991) was used. The accuracy of our measurement is on average 10% depending on the element and concentration, while the precision is around 4%.

The visualization and analysis of particles collected on Nuclepore filter was done using a JEOL 6300 (JEOL, Tokyo, Japan) scanning electron microscope (SEM) equipped with a PGT EDX detector. The detector has a 7.62 μm thick beryllium window, and its energy resolution is 150 eV at 5.9 keV. The conventional single-particle EPMA measurements were carried out at a typical accelerating voltage of 20 kV, and a beam current of 1 nA. The single particles were measured automatically, by scanning the electron beam over the whole projected area of the particles.

The low-*Z* EPMA measurements for the samples collected on metallic foils were carried out on a JEOL 733 electron probe micro-analyzer equipped with an OXFORD energy-dispersive X-ray detector with a super atmospheric thin window (SATW). The resolution of the detector was 133 eV for Mn-Kα X-rays. Measurements on individual particles were carried out automatically as well as manually in the point analysis mode. To achieve optimal experimental conditions, such as low background levels in the spectra and high sensitivity for light element analysis, a 10 kV accelerating voltage was chosen (*Ro et al.*, 1999). In order to minimize the damage of beam sensitive particles such as ammonium sulfate, the measurements were carried out using a liquid-nitrogen-cooled sample stage at a beam current of 1 nA.

Around 100–300 particles were measured in each sample. Morphological parameters such as diameter and shape factor were calculated by the image processing routine of the measuring program. The obtained characteristic X-ray spectra of the particles were evaluated using the AXIL code (*Vekemans et al.*, 1994). Semi-quantitative calculation of the particle composition, including light elements such as C, N and O, was performed by a recently developed approximation method (EP-PROC) (*Osán et al.*, 2000), for the particles collected on metallic foils. The iteration procedure is based on a reverse Monte

Carlo method: in each iteration step, the simulation program calculates the characteristic intensities and a new set of concentration values is determined. Using EP-PROC, the elemental composition of standard particles down to 0.3 μm can be calculated with good agreement between the expected and calculated concentrations (within 3–8% relative) (*Szalóki et al.*, 2000).

3. Results and discussion

3.1 Trace element concentrations

The average and maximum concentrations of trace elements obtained using XRF are shown in *Table 1*, in comparison with the limiting values according to the Hungarian Standard. The obtained concentrations are similar to those found in other areas of Hungary (*Borbély-Kiss et al.*, 1991; *Borbély-Kiss et al.*, 1999), and are in accordance with results obtained by wet chemical methods for the time period of 1995–1998 (*Hlavay et al.*, 2001). The average concentrations are far below the limiting values, and lead is the only element where the maximum concentration is close to the limiting value.

Table 1. Elemental concentrations of TSP samples compared to the limiting values in Hungary

Element	Concentration ($\mu g\ m^{-3}$)		
	Average	Maximum	Limiting value
Al	0.624	1.75	30
Si	1.65	4.96	23.3
P	0.0738	0.149	21.8
S	2.15	5.17	20
Cl	0.0736	0.27	30
K	0.419	1.12	22.6
Ca	1.2	3.38	21.4
Ti	0.042	0.124	n.a.
V	0.00179	0.00724	2
Cr	0.00442	0.0128	1.5
Mn	0.0113	0.0455	1
Fe	0.597	2.14	200
Ni	0.0023	0.00497	1
Cu	0.01	0.0436	2
Zn	0.0384	0.0886	50
Br	0.012	0.0193	10
Rb	0.00271	0.00589	n.a.
Sr	0.0058	0.0128	n.a.
Pb	0.0371	0.106	0.3

There are no large industrial point sources of air pollution near the lake. The nearest power plant, which burns coal, is about 30 km to the northwest. Local sources include motor vehicle emissions and dust suspended by vehicles on paved and unpaved roads or as the result of construction or by wind stress. Leaded gasoline was still widely used in 1995 in Eastern Europe. In Hungary, the lead content of leaded gasoline was decreased to 0.15 g L^{-1} and completely eliminated in April 1999. Some South European countries (e.g., Spain, Italy and Greece), however, asked derogation from the European Union, and they could sell leaded gasoline until the end of 2000. Other heavy metals shown in *Table 1* may originate from oil and coal fired power plants and from waste incinerators. In the former case these emissions are associated with emissions of SO_2, which can be oxidized to sulfate by atmospheric reactions.

3.2 Visualization of particles by SEM

Fig. 1 shows secondary electron images of four typical coarse and fine aerosol particles. By visualizing the samples with SEM, typical particles were found in the coarse fraction as biogenic particles (pollens, spores, algae, plant and insect fragments), crustal particles like aluminosilicates, calcium carbonate and calcium sulfate, as well as salt particles. In the fine fraction, however, irregularly shaped silicates and spherical silicates could be distinguished. The average composition of the particle types in the fine and coarse fractions obtained by single-particle analysis is shown in *Table 2*. A more quantitative description of the different particle types is shown below, in the discussion of the low-Z EPMA results.

3.3 Light element analysis of aerosol particles

In order to obtain information on the possible sources of the aerosol and the possible chemical interactions between gaseous and particulate pollutants, the particles were classified into representative groups using the chemical and morphological data obtained by thin-window EPMA. For comparison of the sample sets collected at different sites and times, all particles for each impactor stage (size fraction) were classified into twelve groups using the non-hierarchical clustering algorithm of Forgy (*Massart* and *Kaufmann*, 1983). The initial centroids for the method were obtained by two steps of hierarchical cluster analysis carried out for each sample using the multivariate statistical software package DPP (*Van Espen*, 1984).

As examples to indicate the differences between small and large particles over Lake Balaton, *Tables 3* and *4* show the classification results for stage 4 and 7, respectively. Particles having an aerodynamic diameter of 0.5–1 μm

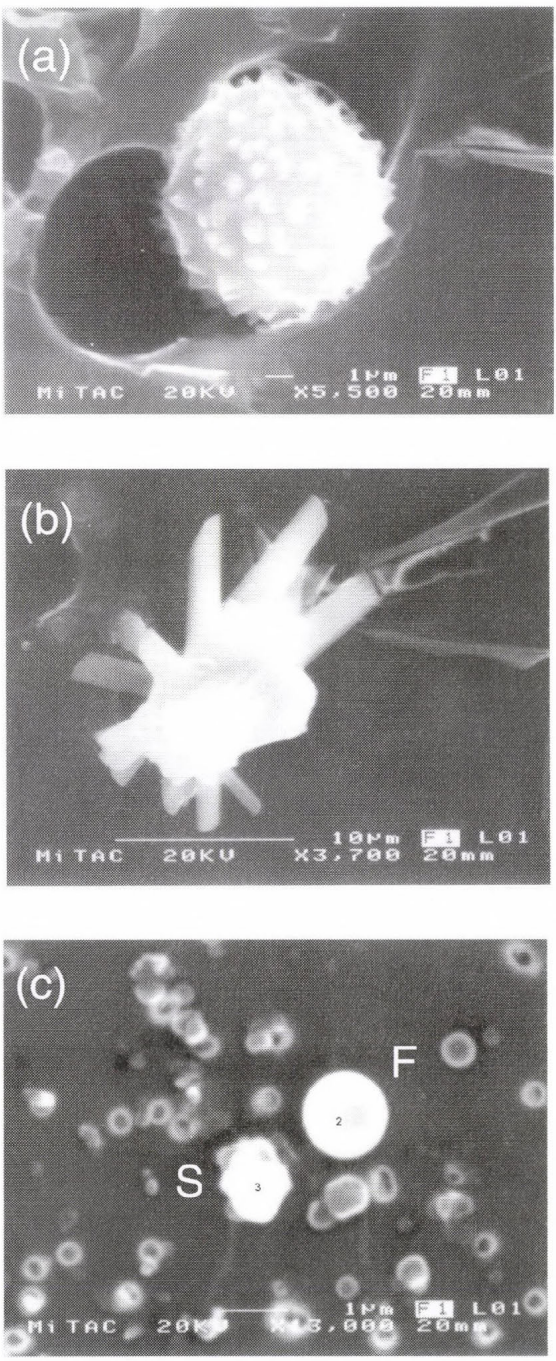

Fig. 1. Secondary electron images of typical aerosol particles collected at Siófok, *(a)* biogenic particle, (*b*) calcium sulfate particle, (*c*) fly-ash (marked as F) and S-rich silicate (marked as S) particle.

were collected on stage 4, while particles with diameters between 4 and 8 μm were collected on stage 7 of the Berner cascade impactor. The majority of the small particles collected on stage 4 are of organic, sulfate and nitrate types. As it can be seen in *Table 3*, the low-Z EPMA method is capable to distinguish different types of sulfur-rich particles, i.e., organic sulfur and ammonium sulfate. The abundance of aluminosilicates is low compared to the larger size fractions, being below 10%.

Table 2a. Average relative X-ray intensity and diameter for the particle types obtained for the stacked filter samples, fine fraction

	Abund.	Diam.	Average relative X-ray intensity (%)											
	(%)	(μm)	Na	Al	Si	S	Cl	K	Ca	Ti	Fe	Cu	Zn	Pb
S-rich	27.6	0.5	0.3	0.0	0.1	98.4	0.0	0.4	0.1	0.0	0.0	0.0	0.2	0.0
Aluminosilicates	19.9	1.1	0.0	20.0	50.1	9.5	0.1	5.5	4.9	0.6	8.2	0.0	0.3	0.0
Fe, S	10.0	0.7	0.0	0.4	3.2	10.9	0.1	0.6	1.4	0.1	79.3	0.2	1.6	0.1
K, S	8.8	0.5	0.6	0.3	2.8	63.8	0.9	20.3	0.7	0.2	4.2	0.6	2.4	0.0
Organic	8.7	0.6	0.1	0.4	0.4	1.3	0.7	0.4	0.3	0.0	0.5	2.0	0.5	0.1
Ca sulfate	7.3	0.7	0.1	0.9	5.6	46.5	0.3	2.0	41.2	0.1	1.9	0.1	0.2	0.0
Quartz	6.2	1.0	0.0	2.1	91.4	3.8	0.1	0.6	0.6	0.1	0.9	0.0	0.0	0.0
Ca-rich	3.7	1.3	0.0	1.2	7.7	6.8	0.8	0.4	76.3	0.0	1.4	0.0	0.1	0.1
K chloride, sulfate	2.5	0.6	0.2	0.0	1.0	12.4	11.4	64.7	1.6	0.2	0.3	0.3	0.4	6.3
Zn, S	1.8	0.5	0.1	0.3	0.5	24.1	0.3	0.2	0.6	0.0	2.8	1.4	62.3	6.8
Pb-rich	1.6	0.5	0.0	0.0	0.2	0.0	0.0	0.2	0.2	0.0	0.0	0.2	1.1	97.6
Cl-rich	1.4	0.5	0.9	0.0	0.9	7.4	74.7	9.9	2.2	0.0	0.0	0.4	0.0	1.9
Ti-rich	0.4	0.7	0.0	2.0	6.1	7.6	0.2	0.1	0.5	79.2	3.2	0.0	0.1	0.0
Na-rich	0.1	0.6	100.0	0.0	0.0	0.0	0.0	0.0	0.0	0.0	0.0	0.0	0.0	0.0

Table 2b. Average relative X-ray intensity and diameter for the particle types obtained for the stacked filter samples, coarse fraction

	Abund.	Diam.	Average relative X-ray intensity (%)											
	(%)	(μm)	Na	Mg	Al	Si	P	S	Cl	K	Ca	Fe	Zn	Pb
Aluminosilicates	31.3	2.9	0.2	0.8	17.6	48.6	0.3	5.6	0.4	6.8	10.7	8.4	0.0	0.0
Ca sulfate	14.2	1.9	0.7	0.7	0.9	4.6	0.6	44.1	1.4	1.5	44.2	1.2	0.1	0.0
Ca-rich	12.7	2.9	0.4	4.0	1.8	9.9	1.2	3.6	1.8	1.2	74.0	1.8	0.0	0.0
Quartz	8.5	2.7	0.2	0.3	3.9	88.0	0.0	1.9	0.1	1.2	2.3	1.9	0.0	0.0
Na, K sulfate	7.6	1.8	4.7	0.6	1.7	8.0	2.0	55.7	1.3	11.5	9.1	3.6	1.1	0.0
S-rich	7.2	1.5	1.7	0.2	0.0	0.6	0.3	92.5	0.0	3.3	0.8	0.3	0.2	0.0
Fe-rich	5.8	2.0	0.1	0.2	0.9	6.2	0.1	6.8	0.4	0.5	3.9	78.0	0.8	0.0
Organic	4.7	1.6	0.5	0.6	0.4	1.5	0.1	1.5	1.8	0.6	1.5	1.0	2.6	0.3
Biogenic	2.9	2.5	0.1	1.0	0.6	3.2	38.3	18.2	6.0	20.6	11.3	0.3	0.1	0.0
Salt	1.7	1.5	9.4	1.0	0.0	0.6	0.2	5.7	75.9	2.5	3.1	0.1	0.6	0.2
Na-rich	1.5	1.5	85.7	0.4	0.0	0.6	0.0	9.0	1.9	0.4	1.8	0.0	0.0	0.0
K-rich	1.1	2.0	0.3	0.4	0.1	2.2	3.9	8.3	4.3	74.2	2.7	0.3	0.3	2.6
Al-rich	0.6	2.2	0.1	0.3	89.6	3.3	0.1	2.6	0.9	0.2	1.5	1.0	0.0	0.0
Pb-rich	0.1	1.1	0.0	0.0	0.0	0.0	0.0	0.0	0.0	2.2	4.1	0.0	2.0	91.7

The time variation of the relative abundance of the particle types obtained is quite high. Although the low-Z EPMA measurements could provide only relative abundances, the significantly high abundance of lead-rich particles observed at the end of September is in agreement with the bulk XRF results showing the maximum lead concentration exactly at that time period. The composition of the "giant" particles collected at stage 7 is different from that of small particles. Crustal particles such as aluminosilicates and calcium carbonate are the most abundant types, followed by biogenic particles. Sulfates, nitrates and salt are less abundant. A high abundance of large ammonium sulfates was observed in September, while small ammonium sulfates were more frequent in the June samples. Sea-salt and aged sea-salt

Table 3a. Average concentration and diameter for the particle types obtained for the samples collected at stage 4 of the Berner impactor

	Abund.	Diam.	Average concentration (wt%)											
	(%)	(μm)	C	N	O	Na	Al	Si	S	K	Ca	Ti	Fe	Pb
Organic + sulfur	20.4	0.9	39.8	8.6	42.8	1.3	0.1	0.1	7.0	0.4	0.0	0.0	0.0	0.0
Organic	15.9	0.9	57.7	4.9	35.6	0.3	0.0	0.0	1.6	0.0	0.0	0.0	0.0	0.0
K sulfate, nitrate	15.1	1.3	8.3	10.6	53.4	0.9	0.0	0.0	14.5	12.2	0.0	0.0	0.0	0.0
Nitrates	9.8	0.6	6.0	10.3	59.3	0.2	0.0	0.2	1.4	0.0	0.0	0.0	22.5	0.0
Ammonium sulfate	9.6	1.0	1.4	6.7	70.2	0.0	0.0	0.0	21.4	0.3	0.0	0.0	0.0	0.0
Aluminosilicates	9.6	1.1	8.3	3.7	54.8	0.0	8.3	20.9	2.1	1.4	0.0	0.0	0.0	0.0
Na sulfate	7.3	0.7	13.2	3.0	52.6	20.3	0.0	0.0	7.3	2.2	0.0	0.0	1.4	0.0
Carbonaceous	4.5	0.9	83.2	0.7	15.8	0.2	0.0	0.0	0.2	0.0	0.0	0.0	0.0	0.0
Ca sulfate	4.2	1.2	10.1	4.4	58.1	0.0	0.6	1.0	5.1	0.0	19.5	0.0	0.0	0.0
Pb-rich	2.1	0.9	3.8	4.8	25.4	0.5	0.0	0.0	5.2	1.9	0.2	0.0	0.0	58.1

Table 3b. Relative abundances (in %) of the obtained particle types in the different samples collected at stage 4 of the Berner impactor

Date of sampling	19	20	16	20	22	23	07	09	11	13	15	20	22	24	25	26	28
	07	07	02	02	02	02	06	06	06	06	06	09	09	09	09	09	09
Origin of air mass			N-	W-		W-	N-	W-		W-				E-			
	n.a.	n.a.	NW	NW	NW	NW	NW	NW	SE	NW	NW	SW	NE	NE	E	E	E
Organic + sulfur	7	21	21	47	25	43	0	5	14	12	7	21	32	19	19	41	17
Organic	2	32	28	6	17	22	0	18	10	3	1	6	33	11	9	18	35
K sulfate, nitrate	3	5	3	21	22	9	9	17	9	6	37	43	10	17	27	16	16
Nitrates	64	6	15	14	16	13	0	3	2	14	1	3	9	0	6	1	4
Ammonium sulfate	11	1	0	2	4	0	81	0	35	2	32	1	1	1	0	1	0
Aluminosilicates	10	11	12	3	3	7	2	14	10	34	15	11	5	3	3	7	6
Na sulfate	0	12	13	3	8	1	0	6	1	10	1	10	2	43	10	3	5
Carbonaceous	1	3	0	1	1	0	1	28	7	3	0	2	4	4	4	9	6
Ca sulfate	2	7	8	3	1	5	0	7	4	11	1	2	3	1	1	0	8
Pb-rich	0	2	0	0	1	0	0	0	0	4	1	1	1	0	21	4	3

particles were observed in the February samples. The original chlorine anion in these particles was substituted by sulfate and/or nitrate through atmospheric reactions with gaseous pollutants (*Kerminen et al.*, 1998).

Table 4a. Average concentration and diameter for the particle types obtained for the samples collected at stage 7 of the Berner impactor

	Abund.	Diam.	Average concentration (wt%)											
	(%)	(μm)	C	N	O	Na	Mg	Al	Si	S	Cl	K	Ca	Fe
Aluminosilicates	26.0	4.6	4.4	3.7	52.0	0.3	2.0	9.3	24.9	0.0	0.0	1.0	2.4	0.0
Ca carbonate	19.2	4.4	5.7	8.1	58.3	0.0	2.3	1.5	2.8	0.1	0.0	0.0	21.1	0.0
Biogenic	13.5	5.6	28.6	11.0	40.3	0.0	0.7	0.0	0.3	0.6	0.0	0.6	17.4	0.0
Ca,Mg sulfate	13.0	4.5	6.8	6.2	62.0	0.9	3.9	0.6	1.4	8.7	0.0	0.0	9.5	0.0
Ammonium sulfate	9.9	5.9	8.7	21.1	54.2	0.1	0.6	0.1	0.0	15.2	0.0	0.0	0.0	0.0
Sodium nitrate	6.5	4.0	0.8	13.3	58.7	21.4	2.5	0.2	0.0	2.3	0.5	0.0	0.4	0.0
Carbonaceous	3.2	5.0	76.1	3.7	19.4	0.0	0.6	0.0	0.1	0.0	0.0	0.0	0.0	0.0
Iron oxide	1.4	3.1	1.1	1.7	33.3	0.0	0.4	0.4	1.0	0.2	0.0	0.0	0.0	61.9
Salt	0.4	2.1	1.7	6.8	24.0	21.0	0.8	0.4	0.4	0.0	44.9	0.0	0.0	0.0

Table 4b. Relative abundances (in %) of the obtained particle types in the different samples collected at stage 7 of the Berner impactor

Date of sampling	19 07	20 07	16 02	18 02	20 02	22 02	23 02	07 06	09 06	11 06	13 06	15 06	20 09	22 09	24 09	25 09	26 09	28 09
Origin of air mass			N-		W-		W-	N-	W-		W-				E-			
	n.a.	n.a.	NW	NW	NW	NW	NW	NW	NW	SE	NW	NW	SW	NE	NE	E	E	E
Aluminosilicates	32	41	40	15	25	32	39	12	59	57	54	17	18	28	4	15	21	38
Ca carbonate	39	34	28	12	32	31	23	26	27	28	34	31	15	9	1	3	7	33
Biogenic	12	14	12	13	8	5	5	15	9	6	6	13	24	11	16	18	24	17
Ca,Mg sulfate	9	7	1	7	7	19	12	12	2	4	3	30	15	40	8	27	12	4
Ammonium sulfate	1	0	0	3	7	3	4	2	0	0	0	0	2	4	66	23	31	0
Sodium nitrate	7	2	4	42	18	2	2	29	1	3	1	8	15	2	2	2	1	0
Carbonaceous	0	1	10	2	0	7	13	1	0	2	1	1	10	5	2	5	3	3
Iron oxide	0	1	3	2	0	1	2	1	2	0	1	0	0	0	0	6	1	4
Salt	0	0	2	4	3	0	0	2	0	0	0	0	0	0	0	0	0	0

3.4 Comparison with air mass backward trajectories

Isobaric trajectories have been compiled at the Hungarian Meteorological Service for the 850 hPa pressure level. It is expected that atmospheric long-range transport processes can be characterized by the wind conditions at that level. In order to determine the possible sources of the aerosol particles, the time variance of the bulk XRF and single-particle EPMA results was studied using principal component analysis. The obtained results were compared to the

850 hPa air mass backward trajectories. The incoming air mass sectors are indicated in *Tables 3* and *4*. During the February campaign, the major components as well as the trace element content did not show significant correlation with the origin of the air mass. For the June and September sampling campaigns, the origin of the air masses could be well explained by the abundance of the particle classes obtained by low-Z EPMA measurements. In June, small sulfate and nitrate particles dominated the samples for marine air masses, and crustal particles were characteristic for trajectories of more continental origin. In September, most of the trajectories crossed Eastern Europe. Large sulfate, nitrate and small lead-rich particles were characteristic for this sampling period. *Fig. 2* shows typical trajectories from June and September 2000.

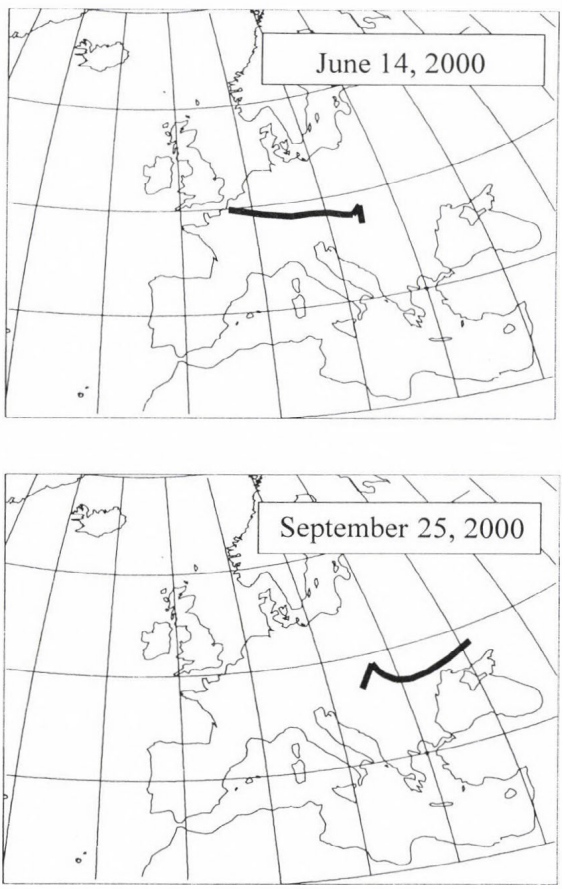

Fig. 2. Air mass backward trajectories calculated for Siófok at the 850 hPa level for 72 h.

4. Conclusions

The combination of bulk XRF and single-particle EPMA combined with cluster and principal component analysis is a powerful tool for characterizing the major, low-Z and trace element composition of atmospheric aerosols. Especially, the low-Z EPMA data were found to be useful for future nutrient deposition calculations for Lake Balaton. The comparison of the analytical data set with air mass backward trajectories yielded good correlation for the sampling periods. The composition of the aerosol did not show characteristic seasonal variation, it was more correlated to the origin of the incoming air mass.

Acknowledgements—The present work was partially supported by the Flemish and Hungarian governments through Joint Project No. B14/98, and by the Hungarian Scientific Research Fund through Project No. OTKA T034195.

References

Borbély-Kiss, I., Bozó, L., Koltay, E., Mészáros, E., Molnár, Á. and *Szabó, Gy.*, 1991: Elemental composition of aerosol particles under background conditions in Hungary. *Atmos. Environ. 25A*, 661-668.

Borbély-Kiss, I., Koltay, E., Szabó, Gy., Bozó, L. and *Tar, K.*, 1999: Composition and sources of urban and rural atmospheric aerosol in Eastern Hungary. *J. Aerosol Sci. 30,* 369-391.

Hlavay, J., Polyák, K. and *Weisz, M.*, 2001: Monitoring of the natural environment by chemical speciation of elements in aerosol and sediment samples. *J. Environ. Monit. 3,* 74-80.

Horváth, L., Mészáros, Á., Mészáros, E. and *Várhelyi, G.*, 1981: On the atmospheric deposition of nitrogen and phosphorus into Lake Balaton. *Időjárás 85,* 194-200.

Kerminen, V.-M., Teinilä, K., Hillamo, R. and *Pakkanen, T.*, 1998: Substitution of chloride in sea-salt particles by inorganic and organic anions. *J. Aerosol Sci. 29,* 929-942.

Massart, D. and *Kaufmann, L.*, 1983: *The Interpretation of Analytical Chemical Data by the Use of Cluster Analysis*. Wiley, New York.

Osán, J., Szalóki, I., Ro, C.-U. and *Van Grieken, R.*, 2000: Light element analysis of individual microparticles using thin-window EPMA. *Mikrochim. Acta 132,* 349-355.

Ro, C.-U., Osán, J. and *Van Grieken, R.*, 1999: Determination of low-Z elements in individual environmental particles using windowless EPMA. *Anal. Chem. 71,* 1521-1528.

Szalóki, I., 1991: Some application of the fundamental parameter method in energy-dispersive X-ray fluorescence analysis by isotope excitation. *X-Ray Spectrom. 20,* 297-303.

Szalóki, I., Osán, J., Ro, C.-U. and *Van Grieken, R.*, 2000: Quantitative characterisation of individual aerosol particles by thin-window EPMA combined with iterative simulation. *Spectrochim. Acta B55,* 1015-1028.

Van Espen, P., 1984: A program for the processing of analytical data (DPP). *Anal. Chim. Acta* 165, 31-49.

Van Malderen, H., Rojas, C. and *Van Grieken, R.*, 1992: Characterization of individual giant aerosol particles above the North Sea. *Environ. Sci. Technol. 26,* 750-756.

Vekemans, B., Janssens, K., Vincze, L., Adams, F. and *Van Espen, P.*, 1994: Analysis of X-ray spectra by iterative least squares (AXIL): New developments. *X-Ray Spectrom. 23,* 278-285.

IDŐJÁRÁS

Quarterly Journal of the Hungarian Meteorological Service
Vol. 105, No. 3, July–September 2001, pp. 157–164

Extreme temperature and precipitation years in Hungary during last century

István Matyasovszky

Department of Meteorology, Eötvös Loránd University,
P.O. Box 32, H-1518 Budapest, Hungary; E-mail: matya@ludens.elte.hu

(Manuscript received March 12, 2001; in final form June 26, 2001)

Abstract—A particular year is called extreme when the actual annual course of a climatic element differs substantially from the average annual course. This concept considers both the magnitude and length of departures from normal. A methodology to measure the difference between an actual and the average year is discussed. The procedure is applied to monthly mean temperatures and monthly precipitation amounts using ten locations in Hungary with homogeneous data sets from 1901 to 1999. Trends of above mentioned differences are analyzed. The chance for extreme years in overall decreases during last century, but there exists a slight tendency of more extreme years from the eighties. The most extreme temperature and precipitation years do not appear simultaneously.

Key-words: extreme year, temporal change, temperature, precipitation.

1. Introduction

Detection and estimation of climatic changes in observed data series have a long history. Data analysis is mainly based on variations of mean, i.e., much of these works applies particular versions of trend models (*Zheng* and *Basher*, 1999). However, several other statistical properties may vary during a changing climate. For instance, long-term change of extremes is an especially important issue for its socio-economic impacts.

The term extreme can be defined by several ways. A typical example is to estimate the probability distribution of the maximum of a climatic element during a given period. Here separate entire years are analyzed and a particular year is called extreme when the actual annual course differs substantially from the average annual course. This concept considers both the magnitude and length of departures from normal.

A methodology to measure the difference between an actual and the average year is discussed in Section 2. The procedure is applied to monthly mean temperatures and monthly precipitation amounts using ten locations in Hungary with homogeneous data sets from 1901 to 1999. Trends of above mentioned differences are analyzed with linear and non-parametric regression techniques in Section 3. Finally a brief section for conclusions is provided.

2. Methodology

A methodology for extremes of multivariate time series has been developed by *Szentimrey* (1999), the present technique is a specific version of his general procedure. The task is to define a quantity to measure the deviation of actual annual courses from the average annual course in the area considered. When this quantity is large, that year can be called extreme. Let $x(i,j)=(x_1(i,j),\ldots,x_K(i,j))^T$ be a vector representing monthly mean temperature or monthly precipitation amount at K locations for jth month in ith year where T denotes the transpose. In order to characterize the spatial distribution a principal component analysis is used. Only the first principal component is preserved, because it explains a large portion of the total variance of K variables due to the small area examined. This new variable is calculated as

$$y(i,j)=\mathbf{u}^T\,\mathbf{x}(i,j), \tag{1}$$

where $\mathbf{u}$ is the eigenvector corresponding to the largest eigenvalue of the matrix consisting of correlations among locations. To estimate these correlations a standardization

$$x_k^*(i,j)=\frac{x_k(i,j)-m_k(j)}{d_k(j)} \tag{2}$$

is introduced, because means and standard deviations change from month to month. Here $m_k(i,j)$ and $d_k(i,j)$ are means and standard deviations, respectively. Denoting the number of months by $J=12$ and having a data set which covers I years, the means and variances are replaced by their empirical values calculated as

$$\hat{m}_k(j)=\bar{x}_k(j)=\frac{1}{I}\sum_{i=1}^{I}x_k(i,j), \qquad \hat{d}_k^2(j)=\frac{1}{I-1}\sum_{i=1}^{I}(x_k(i,j)-\bar{x}_k(j))^2. \tag{3}$$

Since the covariance matrix of standardized variables is identical to the correlation matrix of original variables, the correlation r_{pq} between pth and qth locations is estimated by

$$r_{pq} = \frac{1}{IJ} \sum_{i=1}^{I} \sum_{j=1}^{J} x_p^*(i,j)\, x_q^*(i,j). \tag{4}$$

Note that temporal variation of these correlations within the year is assumed insignificant. Because the variable $y(i,j)$ has different variances in different months, larger deviations from mean can be expected in months having larger variances. Therefore, a further normalization is needed next. Taking empirical means $\bar{\mu}_j$ and standard deviations $\bar{\delta}_j$ of $y(i,j)$, an additional standardization is performed as

$$z(i,j) = \frac{y(i,j) - \bar{\mu}_j}{\delta_j}. \tag{5}$$

Finally, a norm $\|\mathbf{z}(i)\|^2$ should be introduced to quantify the deviation of actual annual courses from the average annual course, where $\mathbf{z}(i) = (z_1(i),..., z_J(i))^T$. Since components of the vectors $\mathbf{z}(i)$ are not statistically independent, a Euclidian norm is not very useful. Therefore, principal components of vectors $\mathbf{z}(i)$ are determined and the Euclidean squared norms

$$s(i) = \|\mathbf{w}(i)\|^2 = \mathbf{w}(i)^T \mathbf{w}(i) \tag{6}$$

with new uncorrelated variables are calculated, where

$$\mathbf{w}(i) = \Lambda^{-1/2}\, \mathbf{V}^T \mathbf{z}(i). \tag{7}$$

$\mathbf{\Lambda}$ is a diagonal matrix consisting of eigenvalues of the covariance matrix $\mathbf{C}$ of $\mathbf{z}(i)$ and columns of $\mathbf{V}$ includes eigenvectors corresponding to their eigenvalues. The (p,q)th element of $\mathbf{C}$ is estimated by

$$\hat{c}_{pq} = \frac{1}{I} \sum_{i=1}^{I} z_p(i)\, z_q(i). \tag{8}$$

3. Results

Monthly mean temperatures and monthly precipitation amounts are examined using data of ten stations, namely Budapest (KMI), Debrecen, Kecskemét, Miskolc, Mosonmagyaróvár, Nyíregyháza, Pécs, Sopron, Szeged and Szombathely. Data sets have been homogenized by *Szentimrey* (1999) and are available for the period from 1901 to 1999.

When applying a principal component analysis, the first principal component explains 94.5% of the total variance for temperature and 58.2% for precipitation. Using the procedure described in previous section, the first ten largest norms Eq. (6) were selected for both the temperature and precipitation. Also, a similar analysis was performed when the two elements were handled together, i.e., the dimension K is twice of locations according to temperature and precipitation of each station. Temporal distributions of these extreme years are shown in *Fig. 1*. In order to compare the magnitude of extremity the values are divided by two when both elements are considered together. An important conclusion is that extreme temperature and precipitation years take place separately, none of extreme years with respect to one element is extreme with respect to other element. In the joint case the source of large deviations from mean annual course is the temperature in four years (1902, 1929, 1940, 1946), while the precipitation is responsible in four other years (1914, 1922, 1936, 1947). Only two years with seventh and eighth largest norms are not extremes with respect to temperature or precipitation alone.

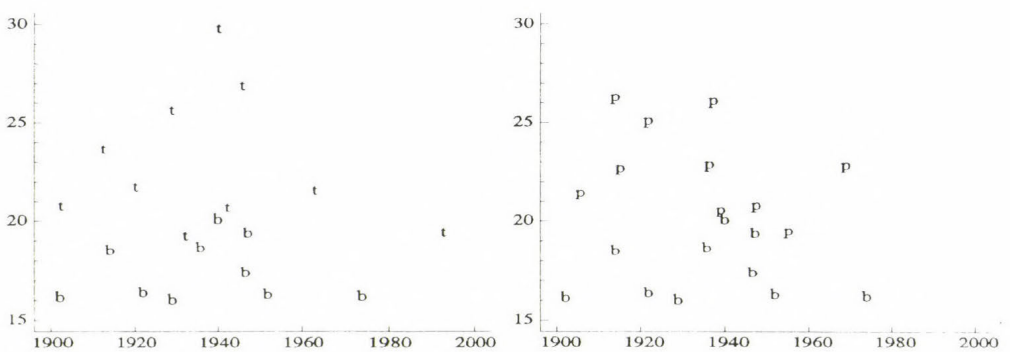

Fig. 1. Temporal distribution of extreme years: *t*- temperature, *p*- precipitation, *b*- both the temperature and precipitation. Vertical axis corresponds to squared norm Eq. (6).

An important question whether norms show temporal changes. Using a linear trend analysis for temperature a chance for decreasing deviations from mean annual course is detected, but the change is significant at only a

relatively weak 10% level. Allowing the trend to be not linear, a non-parametric technique discussed by *Matyasovszky* (1998) was also applied.

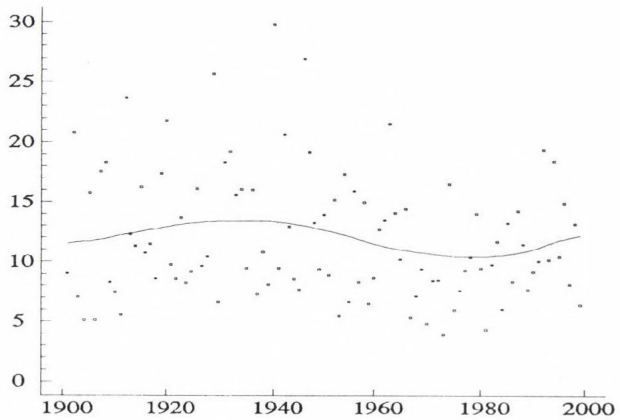

Fig. 2. Trend of squared norm Eq. (6) for temperature.

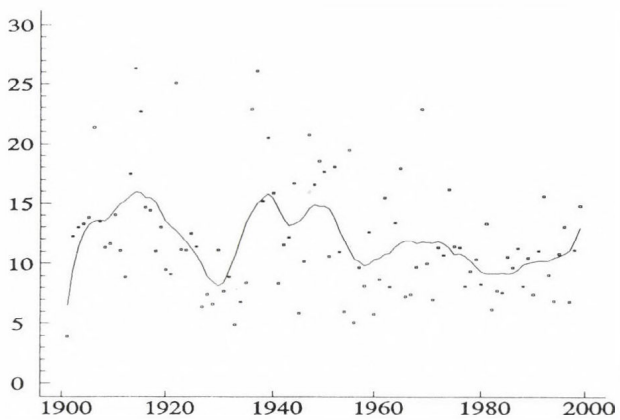

Fig. 3. Trend of squared norm Eq. (6) for precipitation.

Fig. 2 shows a decreasing tendency from forties to eighties and an increasing until forties and during the last two decades. Extremity of the annual course of precipitation is decreasing, because the linear trend is significant at a 2% level. The non-parametric technique results in a highly complicated form of trend showing that precipitation has no long term changes but fluctuates intensively on short time scales (*Fig. 3*). When analyzing the two elements together, a negative linear trend is significant at even a 0.4% level. The norm is essentially constant

until the end of forties but strongly decreases from these years. A slight increase of extremity can be observed in the last two decades (*Fig. 4*).

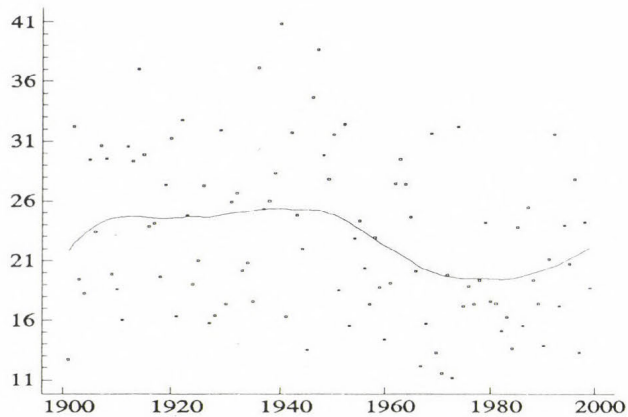

Fig. 4. Trend of squared norm Eq. (6) for temperature and precipitation together.

A natural way to describe the annual course is to use a discrete Fourier transform of data, i.e.,

$$z^*(i,j) = a_{i0} + \sum_{m=1}^{M} a_{im} \cos\left(\frac{2\pi mj}{J}\right) + \sum_{m=1}^{M-1} b_{im} \sin\left(\frac{2\pi mj}{J}\right), \tag{9}$$

where

$$z^*(i,j) = \frac{y(i,j) - \hat{\mu}_j}{\hat{\delta}_j} + \hat{\mu}_j, \tag{10}$$

$$a_{i0} = \frac{1}{J} \sum_{j=1}^{J} z(i,j), \tag{11}$$

$$a_{im} = \frac{2}{J} \sum_{j=1}^{J} z(i,j) \cos\left(\frac{2\pi mj}{J}\right), \qquad m = 1,\ldots,M, \tag{12}$$

$$b_{im} = \frac{2}{J} \sum_{j=1}^{J} z(i,j) \sin\left(\frac{2\pi mj}{J}\right), \qquad m = 1,\ldots,M-1, \tag{13}$$

and $M=J/2$. Temporal variations are mainly characterized by the annual cycle corresponding to $m=1$. Therefore, the amplitudes $\left(c_{i1}^2 = a_{i1}^2 + b_{i1}^2\right)^{1/2}$ are ana-

lyzed with linear and nonparametric regression techniques. For temperature, linear trend is not statistically significant at any reasonable level, but the nonparametric procedure results in considerable changes. The curve in *Fig. 5* is highly similar to the curve in *Fig. 2*. Smallest amplitudes in eighties correspond to warm winters and mild summers, while largest values in forties characterize principally cold winters. Note that two of the first ten largest norms take place during these years (*Fig. 1*). Extreme years are generally cold rather than warm especially during winters. To illustrate this fact *Fig. 6* shows the average annual course and the first four most extreme annual courses.

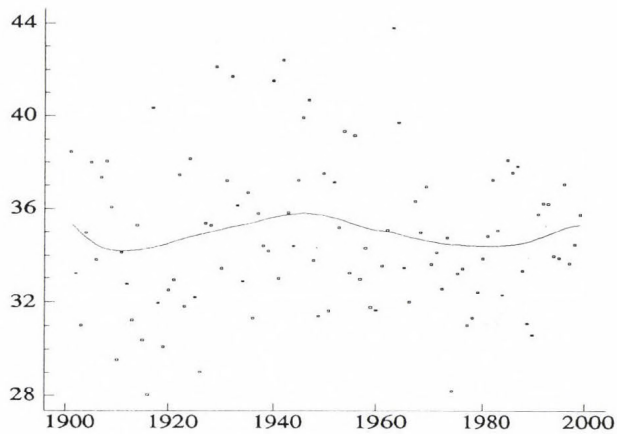

Fig. 5. Trend of annual cycle of the first principal component of monthly mean temperatures.

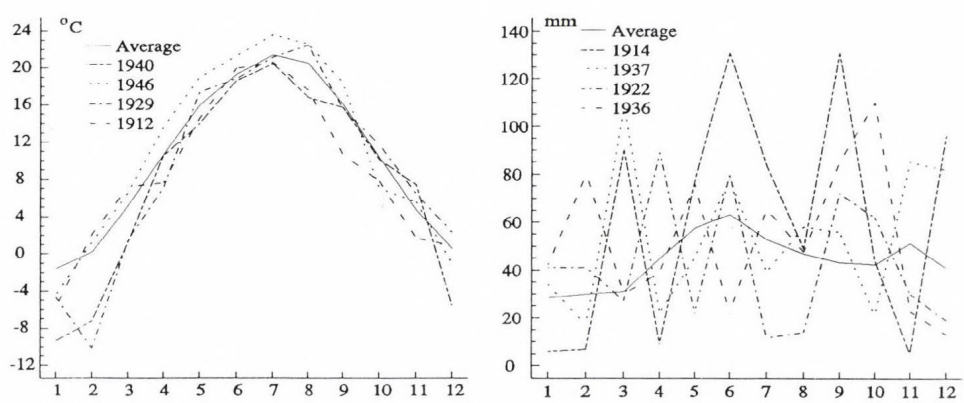

Fig. 6. First four most extreme temperature (*a*) and precipitation (*b*) years in Kecskemét.

Every curve is below the average in January and the cold period continues until middle of spring in two cases. The cold period is situated in the second half of summer and autumn in 1912. The year 1946 is, however, characterized by warm spring and summer. In case of precipitation no any trend of the annual cycle can be detected due to larger variability within the year. The most extreme years have a chance to suffer precipitation amounts considerably higher than normal, but the temporal distribution of excessive amounts or shortages appears quite irregular.

4. Conclusions

A norm was defined to measure departures of actual annual courses of monthly mean temperatures and monthly precipitation amounts from average annual courses. Large values of this quantity may identify extreme years. Main conclusions of the analysis of time series of the norm can be summarized as follows:

- Extremity of the annual course of both the temperature and precipitation is characterized by an overall decreasing tendency. A non-parametric regression technique shows a more complex form of trend functions especially for precipitation. The norms slightly increase from the eighties.
- Taking first ten largest norms, only one year follows after the sixties for temperature, while no any year of the last three decades belongs to first ten norms for precipitation.
- When analyzing the two elements together, a negative linear trend is very significant. The norm is essentially constant until the end of the forties but strongly decreases from these years. A slight increase of extremity can be observed in last two decades. Only two years with seventh and eighth largest norms are not extremes with respect to temperature or precipitation alone.

Acknowledgements—Research leading to this paper has been supported by grant from Hungarian Science Foundation OTKA T025803 and Bolyai János scholarship of Hungarian Academy of Sciences.

References

Matyasovszky, I., 1998: Non-parametric estimation of climatic trends. *Időjárás 102*, 149-158.

Szentimrey, T., 1999: Multiple Analysis of Series for Homogenization (MASH). *Proc. of the Second Seminar for Homogenization of Surface Climatological Data,* Budapest, Hungary. WMO, WCDMP-No. 41, 27-46.

Szentimrey, T., 1999: An analysis of extremes of multivariate time series. In *Weather and Climate Extremes* (in Hungarian). Meteorológiai Tudományos Napok 1999, Orsz. Meteorológiai Szolgálat, Budapest, 77-88.

Zheng, X. and *Basher, R.E.*, 1999: Structural time series models and trend detection in global and regional time series. *J. Climate 12*, 2347-2358.

IDŐJÁRÁS

Quarterly Journal of the Hungarian Meteorological Service
Vol. 105, No. 3, July–September 2001, pp. 165–182

The surface aerodynamic transfer parameterization method SAPA: description and performance analyses

Ferenc Ács and **Mihály Kovács**

[1]*Department of Meteorology, Eötvös Loránd University,*
P.O. Box 32, H-1518 Budapest, Hungary; E-mail: acs@caesar.elte.hu

[2]*Department of Applied Analysis, Eötvös Loránd University,*
Kecskeméti u. 10-12, H-1053 Budapest, Hungary

(Manuscript received December 4, 2000; in final form May 25, 2001)

Abstract—The **s**urface **a**erodynamic transfer **pa**rameterization method SAPA is presented. The method is based on the Monin-Obukhov similarity theory describing an implicit equation system of flux/profile relationships. The equation system is solved numerically using fixed-point method. This fixed-point method application is the unique and new feature of the scheme comparing to other schemes. We show that—though an iterative procedure is applied—the method seems to be reliable not only in the common but also in the extrem cases. This is demonstrated analysing the performance of the scheme in terms of both numerical and physical features. We tested also the goodness of the scheme on the Cabauw data set. The method considered can be applied in the land-surface parameterization schemes of weather and climate models.

Key-words: Monin-Obukhov similarity theory, fixed-point method, iterative solution, numerical and physical features of the scheme.

1. Introduction

A large number of surface aerodynamic transfer parameterization methods (SAPA) have been proposed and used in atmospheric modeling. All of these formulations are based on the Monin-Obukhov (M-O) similarity theory which defines an implicite equation system of flux/profile relationships. Such equation systems can be solved either analytically by reformulating the M-O theory in term of bulk Richardson number (*Deardorff*, 1972; *Louis*, 1979; *Byun*, 1990; *Lee*, 1997; *de Bruin et al.*, 2000) or numerically by applying a numeri-

cal procedure (*Schayes*, 1982; *Berkowicz* and *Prahm*, 1982; *Holtslag* and *van Ulden*, 1983; *Manju* and *Scharma*, 1987; *Mohan* and *Siddiqui*, 1998). Today both analytical and numerical approaches are common. Analytical approaches are described in more details. For unstable conditions they yield approximate solutions, that is, the solution can be treated as semi analytical. Description of the numerical approaches is poorer: commonly there are only short remarks concerning the numerical method applied and its performance in the procedure of solution (*Mohan* and *Siddiqui*, 1998).

In this study we present a SAPA method based on the numerical approach. The kernel of the numerical approach is the fix point method. Our basic intention is to show that the fix point method is a powerful numerical procedure for solving the implicitly defined equation system of flux/profile relationships. We analyzed its performance with more attention in terms as follows:

(1) Whether the number of iteration steps depends upon the meteorological conditions. How the equation system converges in both strong unstable and strong stable conditions.

(2) Whether the initial value of Monin-Obukhov's length determines the rate of the convergence.

We analyzed also the basic physical features of the the SAPA method. We estimated its performance on the Cabauw data (*Beljaars* and *Bosveld*, 1997) comparing the calculated and observed turbulent heat fluxes in the intensive observation period. We also analyzed the dependence of friction velocity, aerodynamic resistance and turbulent heat fluxes upon the main forcing factors: the surface-air temperature difference and the wind velocity. This study is a revised and updated text of the lecture presented as poster (*Kovács* and *Ács*, 2000) at the 25th General Assembly of the European Geophysical Society.

2. Method

The SAPA method is based on the Monin-Obukhov similarity theory considering an implicit equation system of flux/profile relationships. The equation system is solved by the fixed-point method. The method is used as turbulent heat flux parameterization module in the Psi1-PROGSURF model (*Ács* and *Hantel*, 1998). In the following both numerical procedure and physical background will be presented in detail.

2.1 *Basic equations*

2.1.1 *Turbulent heat fluxes*

The turbulent heat fluxes are calculated by aerodynamic formulae. The latent heat flux is parameterized as:

$$\lambda \cdot E^j = -\frac{\rho c_p}{\gamma} \frac{f^j \cdot e_S(T_{vg}) - e_r}{r_a^j + r^j}, \tag{1}$$

where ρ is the air density, c_p is the specific heat of air at constant pressure, γ is the psychrometric constant, $e_S(T_{vg})$ is the saturation vapor pressure at the vegetation-ground temperature T_{vg}, e_r is the vapor pressure at reference level, r_a is the aerodynamic resistance and r is the surface resistance. The superscript j refers to the domains of vegetation ($j = v$) and of bare soil ($j = b$). For vegetation we additionally distinguish between wet ($j = vw$) and dry ($j = vd$) vegetation surface. As a first approach in both cases we put

$$f^{vw} = f^{vd} = 1. \tag{2}$$

f^b represents the relative humidity on the bare soil surface. It is parameterized after *Noilhan* and *Planton* (1989) as

$$f^b = \begin{cases} 1 & if \quad \theta_{f1} \le \theta_1 \\ 0.5 \cdot \{1 - \cos(\theta_1 \cdot \pi / \theta_{f1})\} & if \quad \theta_{w1} \le \theta_1 < \theta_{f1} \\ 0 & if \quad \theta_1 \le \theta_{w1} \end{cases}, \tag{3}$$

where θ_1 represents actual soil moisture content. θ_{f1} and θ_{w1} is the field capacity and wilting point soil moisture content in the surface layer (m^3/m^3), respectively.

The sensible heat flux is parameterized as:

$$H^j = -\rho c_p \frac{T_{vg} - T_r}{r_a^j}, \tag{4}$$

where T_r is air temperature at the reference level.

2.1.2 Aerodynamic resistances

The aerodynamic resistance is divided into laminar and turbulent terms.

- Vegetation: $r_a^v = r_{al}^v + r_{at}^v$. (5)
- Bare soil: $r_a^b = r_{al}^b + r_{at}^b$. (6)

2.1.3 Laminar component

This term is generally not negligible and in many cases it is even larger than the turbulent aerodynamic resistance component.

Vegetation
Above vegetation, the aerodynamic resistance for heat transfer in the laminar layer is parameterized combining the expression of *Wetzel* and *Chang* (1988) and the so called excess resistance term:

$$r_{al}^v = \frac{5}{u_*} + 6 \cdot u_*^{-2/3}. \tag{7}$$

The first term characterizes the laminar layer resistance for momentum transfer, the second one expresses the deviation between the momentum and heat transfer mechanisms close to the vegetation surface. u_* is the friction velocity.

Bare soil
In the immediate vicinity of bare soil surface, there are no fundamental differences between the momentum and heat transfer mechanisms, therefore,

$$r_{al}^b = \frac{5}{u_*}. \tag{8}$$

2.1.4 Turbulent component

The turbulent component of aerodynamic resistance r_{at} is evaluated using Monin-Obukhov's similarity theory taking into account the atmospheric stability.

Parameterization of turbulent component will not be considered separately for vegetation and bare soil. The parameters which are different for vegetation and bare soil are as follows: D_{Stherm}, D_{Sdyn} and z_0. All three parameters are defined below (Eqs. (14), (17) and (15)).

- **Resistance**

The turbulent aerodynamic resistance is defined as follows:

Neutral stratification

$$r_{at} = \frac{0.74}{k \cdot u_*} \cdot \log\left(\frac{D_{Stherm}}{z_0}\right). \tag{9}$$

Stable stratification

$$r_{at} = \frac{1}{k \cdot u_*}\left[0.74 \cdot \log\left(\frac{D_{Stherm}}{z_0}\right) + 4.7 \cdot \chi \cdot (D_{Stherm} - z_0)\right]. \tag{10}$$

Unstable stratification

$$r_{at} = \frac{0.74}{k \cdot u_*} \cdot \log\left(\frac{1 - t_r}{1 - t_0} \cdot \frac{1 + t_0}{1 + t_r}\right), \tag{11}$$

with functions:

$$t_r = \left[1 - 9 \cdot D_{Stherm} \cdot \chi\right]^{-1/2}, \tag{12}$$

$$t_0 = \left[1 - 9 \cdot z_0 \cdot \chi\right]^{-1/2}. \tag{13}$$

k is von Kármán constant, $\chi = \frac{1}{L}$ and L is Monin-Obukhov length. Coefficient 0.74 appears in Businger's universal functions (*Ács et al.*, 2000). Thickness of layer D_{Stherm} differs above vegetation and bare soil, that is

$$D_{Stherm} = \begin{cases} z_{rtherm} & for\ bare\ soil \\ z_{rtherm} - d & for\ vegetation \end{cases}. \tag{14}$$

z_{rtherm} is the reference level for air temperature and humidity and d is the zero plane displacement height (m). d can be either estimated via vegetation morphological characteristics or prescribed as in this study. z_0 is the roughness length (m); it differs for vegetation and bare soil, that is

$$z_0 = \begin{cases} z_0^b & \textit{for bare soil} \\ z_0^v & \textit{for vegetation} \end{cases}. \tag{15}$$

χ is the stability wavenumber.

- **Friction velocity**

The friction velocity is defined by:

$$u_* = \frac{k \cdot U_r}{\log\left(\frac{D_{Sdyn}}{z_0}\right) - \Psi_m}, \tag{16}$$

where thickness of layer D_{Sdyn} is calculated by

$$D_{Sdyn} = \begin{cases} z_{rdyn} & \textit{for bare soil} \\ z_{rdyn} - d & \textit{for vegetation} \end{cases}. \tag{17}$$

Ψ_m is the stability function which depends upon $D_{Sdyn} \cdot \chi$; U_r is the wind speed at the wind's reference level z_{rdyn}.

- **Stability function**

Stability function depends upon stratification.

Neutral stratification

$$\Psi_m = 0. \tag{18}$$

We use two different entries for the argument of Ψ_m. When $D_{Sdyn} \cdot \chi \leq 0.5$ we enter the empirical expression of *Businger et al.* (1971):

$$\Psi_m = -4.7 \cdot D_{Sdyn} \cdot \chi. \tag{19}$$

For $D_{Sdyn} \cdot \chi > 0.5$ we use the formula of *Holtslag* and *de Bruin* (1988):

$$\Psi_m = -A \cdot D_{Sdyn} \cdot \chi - B \cdot \left(D_{Sdyn} \cdot \chi - \frac{C}{D} \cdot e^{-D \cdot D_{Sdyn} \cdot \chi} \right) - \frac{B \cdot C}{D} \tag{20}$$

with $A = 0.7$, $B = 0.75$, $C = 5$ and $D = 0.35$.

Unstable stratification

$$\Psi_m = 2 \cdot \log\left(\frac{1+x}{2} \right) + \log\left(\frac{1+x^2}{2} \right) - 2 \cdot \arctan(x) + \frac{\pi}{2}, \tag{21}$$

with the x function proposed by *Businger et al.*, (1971),

$$x = \left[1 - 16 \cdot D_{Sdyn} \cdot \chi \right]^{1/4}. \tag{22}$$

- **Stability wavenumber**

Stability wavenumber is defined by

$$\chi = \frac{1}{L}, \tag{23}$$

where L is the Monin-Obukhov length defined by

$$L = \frac{\rho \cdot T_r \cdot u_*^3}{g \cdot k \cdot \left(\frac{H}{c_p} + 0.61 \cdot T_r \cdot E \right)}, \tag{24}$$

where g is the acceleration of gravity (m s^{-2}) and E is the vapor flux (kg m^{-2} s^{-1}).

Neutral stratification is supposed for $|L| > 800$ m that is $\chi < 0.00125$ m^{-1}. If the stratification is not neutral, it is stable (L or $\chi > 0$) or unstable (L or $\chi < 0$).

2.2 Solving procedure

The stability wave number depends upon E, H and u_*, and vice versa. The chain of formulae involved is Eq. (23), Eq. (24) for χ and L; Eq. (1) for E; Eq. (4) for H; Eqs. (5) and (6) for r_a; Eq. (16) for u_*; Eqs. (18), (19) and (21) for Ψ_m which leads back to χ. Symbolically:

$$\chi = F\left\{E\left[r_a^j\left(u_*[\Psi_m(\chi)]\right)\right],\ H\left[r_a^j\left(u_*[\Psi_m(\chi)]\right)\right],\ u_*[\Psi_m(\chi)]\right\}. \tag{25}$$

Implementing all functional relationships and parameterizations with external conditions into Eq. (25) this reads:

$$\chi = F(\chi, bc)\,, \tag{26}$$

where

$$F(\chi,bc) = F\left\{E\left[r_a^j\left(u_*[\Psi_m(\chi),bc],bc\right),bc\right],H\left[r_a^j\left(u_*[\Psi_m(\chi),bc],bc\right),bc\right],u_*[\Psi_m(\chi),bc]\right\}. \tag{27}$$

bc represents external conditions involved in the various parameterizations (for example, the reference temperature or the wind speed). They are assumed constant. The implicit equation, Eq. (26) is solved by the fixed-point method. According to numerous tests the method always seems to be convergent. A short description of the method is presented in the Appendix. The χ and $F(\chi)$ functions for defined external conditions are presented in *Fig. 1*. As it can be seen, it yields exactly one χ^* solution (χ^* is the cross point of χ and $F(\chi,bc)$ functions) for the unstable, neutral and stable conditions. The χ^* solution is obtained iteratively fulfilling the $|\chi - F(\chi,bc)| \le 10^{-4}$ condition.

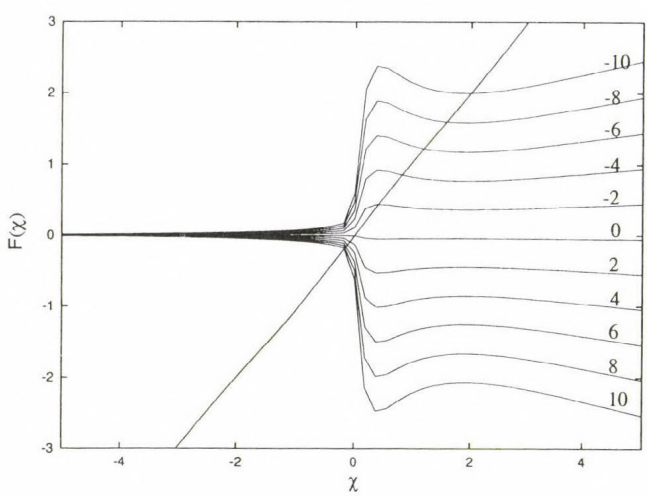

Fig. 1. The shape of $F(\chi)$ function obtained by SAPA. The curves refer to the following atmospheric forcing data: U_r = 2.0 m s^{-1}, relative humidity RH = 90 per cent, T_{vg} = 20°C and T_r varied from 10°C to 30°C in steps of 2°C. The numbers on the curves represent $T_{vg} - T_r$ values.

3. Results

First, the numerical features of the fixed-point method are investigated. Then we tested the scheme using Cabauw data set. Lastly, we analyzed the dependence of the friction velocity, aerodynamic resistance and the turbulent heat fluxes upon main forcing factors.

3.1 Numerical features

The results show that the number of the iteration steps N_i depends upon the meteorological conditions (*Fig. 2*). Usually N_i is less than 10 for both moderately stable and unstable conditions. But, in general, stable condition needs more iteration than the unstable one. N_i is determined by the wind velocity in the greatest extent. For strong unstable conditions, close to or at the boundary of free convection zone (extremely small wind and great surface/air temperature difference), there are cases when N_i is greater than 200. Similarly, for strong stable conditions with small winds (U_r is about or less than 1 m s^{-1}), N_i is about 100 or still greater. It is interesting to note that in these conditions the field of N_i shows maxima.

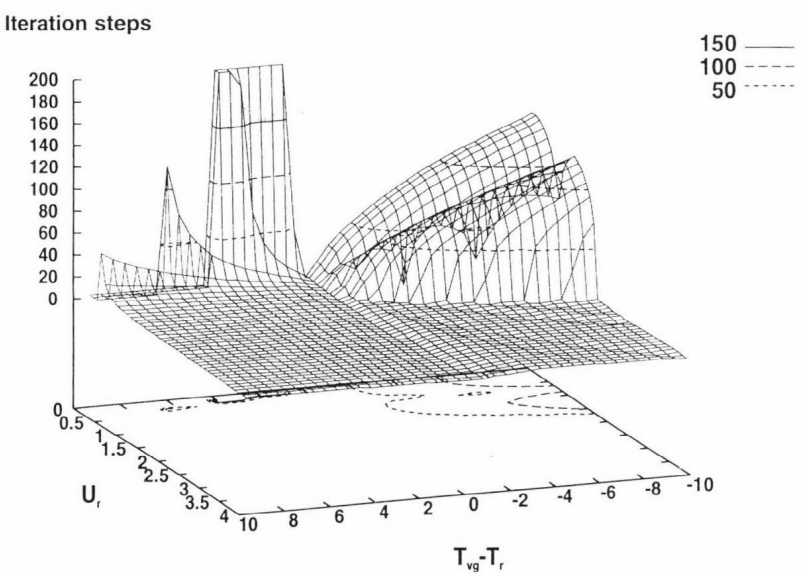

Fig. 2. The number of the iteration steps versus different wind velocity and temperature difference values $T_{vg} - T_r$ for small vegetation surface resistance (r^v = 60 s m^{-1}) and RH = 90 per cent.

The initial values of χ determine the rate of the convergence. This is shown with the aid of *Figs. 3* and *4*. *Fig. 3* refers to small winds ($U_r = 0.1$ m s^{-1}). Here in stable conditions there is such initial χ_0 value (about 2 m^{-1}), for which N_i would be considerably smaller. In spite of this, for average wind conditions ($U_r = 4$ m s^{-1}) there is no such initial χ_0 value. This is shown in *Fig. 4*.

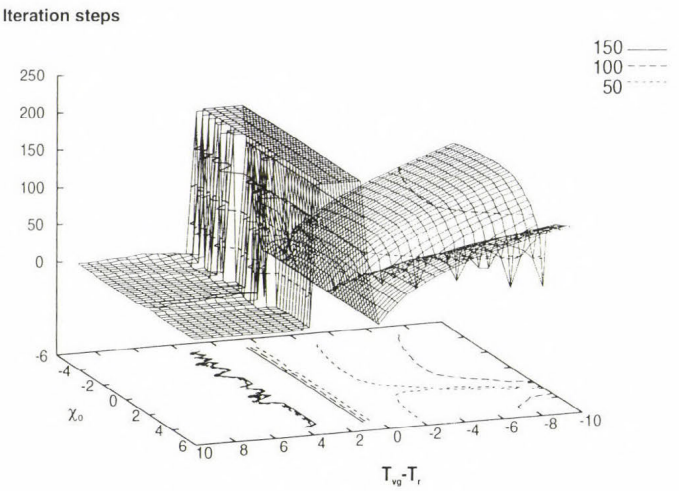

Fig. 3. The number of the iteration steps versus the initial values of χ and the temperature differences $T_{vg} - T_r$ for small vegetation surface resistance ($r^v = 60$ s m^{-1}) and $U_r = 0.1$ m s^{-1}.

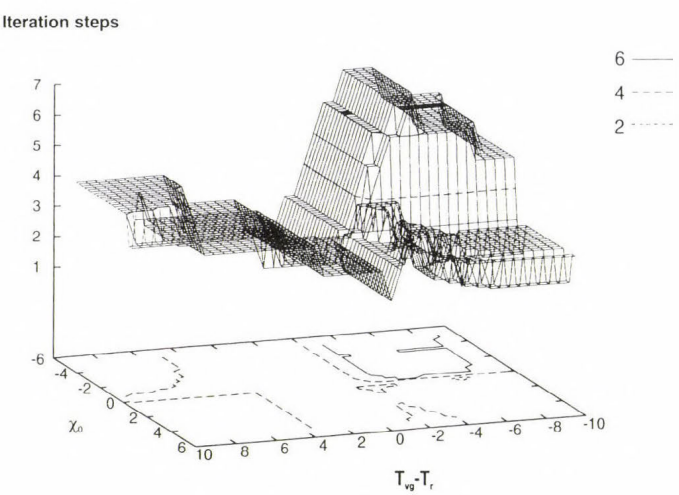

Fig. 4. As Fig. 3 but for $U_r = 4$ m s^{-1}.

3.2 Validation experiments

The scheme is tested by comparing simulated and observed turbulent heat fluxes. The well known 1987 data from Cabauw, The Netherlands, are used. Cabauw site has a humide, maritime climate. The soil texture in the root zone is silty clay. The plant cover is mainly short grass.

The data set contains also instantaneous values of turbulent heat fluxes measured in the intensive observation period between September 10–19, 1987. The comparison of simulated and observed latent and sensible heat fluxes is presented in *Figs. 5* and *6*. The results obtained are reliable. The agreement is somewhat better for λE than for H. The correlation coefficients obtained are 0.82 and 0.71, respectively. In these tests SAPA is used as submodule in the scope of Psil-PROGSURF (*Ács* and *Hantel*, 1998).

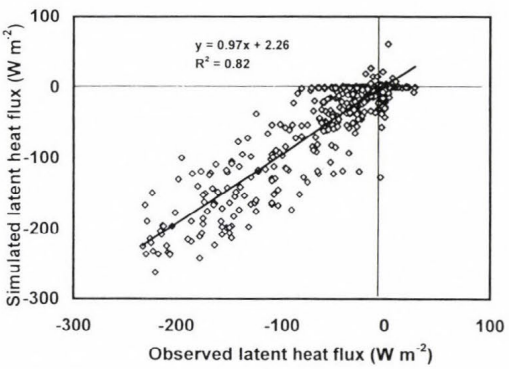

Fig. 5. SAPA-simulated versus observed latent heat flux in the intensive observation period (from day 253 to day 262). Thick line: regression.

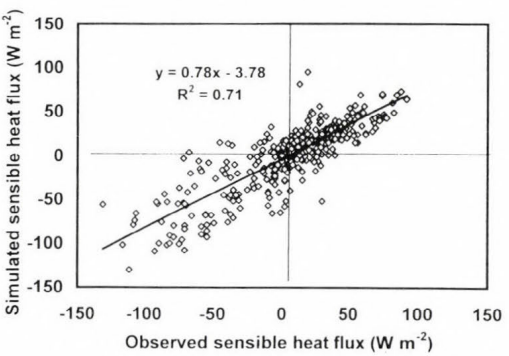

Fig. 6. SAPA-simulated versus observed sensible heat flux in the intensive observation period (from day 253 to day 262). Thick line: regression.

3.2 Physical features

The performance of SAPA is also briefly analyzed in terms of fields of $r_a(T_{vg} - T_r, U_r)$, $u_*(T_{vg} - T_r, U_r)$, $\lambda \cdot E(T_{vg} - T_r, U_r)$ and $H(T_{vg} - T_r, U_r)$. Vegetation surface is choosen. The vegetation surface resistance is small, that is $r^v = 60$ s m^{-1}. The vegetation type is short grass. Note, that these surface conditions are very similar to the conditions on the Cabauw site. The atmospheric boundary conditions are as follows: The $T_{vg} - T_r$ temperature difference is changed between -10 and $+10$°C. This is achieved by $T_{vg} = 20$°C and changing T_r from 10°C to 30°C in steps of 0.5°C. U_r is varied from 0.1 to 4.0 m s^{-1} in steps of 0.1 m s^{-1}. The relative humidity of air RH is constant. In the so called "wet case" RH is 90 per cent, in the "dry case" RH is 30 per cent. It has to be noted that in the simulations the moisture state of the surface (represented by r^v) and the surface/air temperature difference (represented by $T_{vg} - T_r$) are independent from each other.

The fields of r_a^v, u_*, $\lambda \cdot E$ and H are presented in *Figs. 7, 8, 9* and *10*, respectively. The "wet" and "dry" case are distinguished by notation a and b, respectively. The basic characteristics of the fields are as follows:

(1) In all cases three stability regimes can be recognized: the stable stratification, the unstable stratification and the free convection zone. Note that the free convection zone (region of small winds and great positive surface/air temperature differences) can be recognized though the universal functions for unstable stratification (Eqs. (12), (13) and (22)) are used.

(2) There is no qualitative difference between the fields of r_a^v, u_*, $\lambda \cdot E$ and H for "wet" ($RH = 90$ per cent) and "dry" ($RH = 30$ per cent) cases. The deviation between the "wet" and "dry" case seems to be more pronounced for $\lambda \cdot E$ field. In "dry" case the change of $\lambda \cdot E$ versus $T_{vg} - T_r$ is more pronounced than in the "wet" case.

(3) The fields of u_*, $\lambda \cdot E$ and H are basically similar. It can be said that the form of u_* field governs in great extent the form of $\lambda \cdot E$ and H fields. The form of r_a^v field does not follow the form of u_* field. r_a^v can be treated as an opposite of u_*. In the regions where u_* has a minimum, r_a^v appears with the maximum and vice versa.

Let us inspect each figure separately in more details. We will describe the fields of "dry" case.

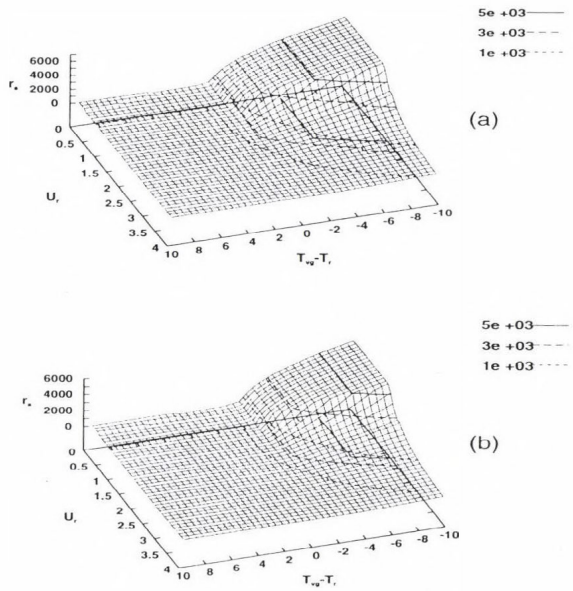

Fig. 7. The aerodynamic resistance versus the surface/air temperature difference $T_{vg} - T_r$ and the wind velocity for (*a*) $RH = 90$ per cent ("wet" case) and (*b*) $RH = 30$ per cent ("dry" case).

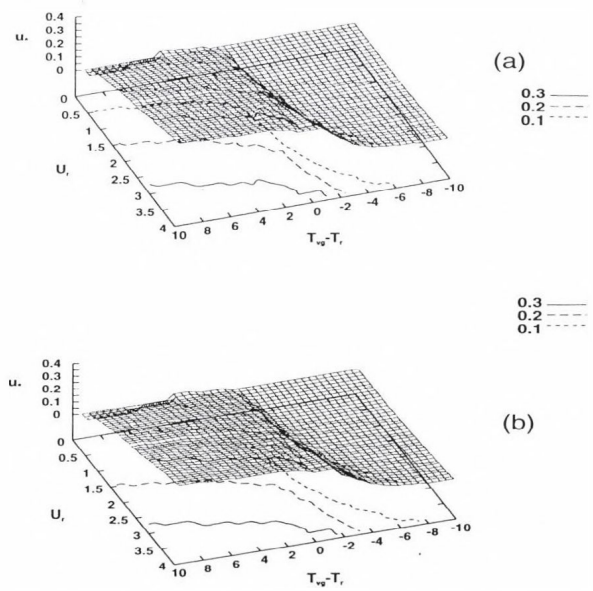

Fig. 8. The friction velocity versus the surface/air temperature difference $T_{vg} - T_r$ and the wind velocity for (*a*) $RH = 90$ per cent ("wet" case) and (*b*) $RH = 30$ per cent ("dry" case).

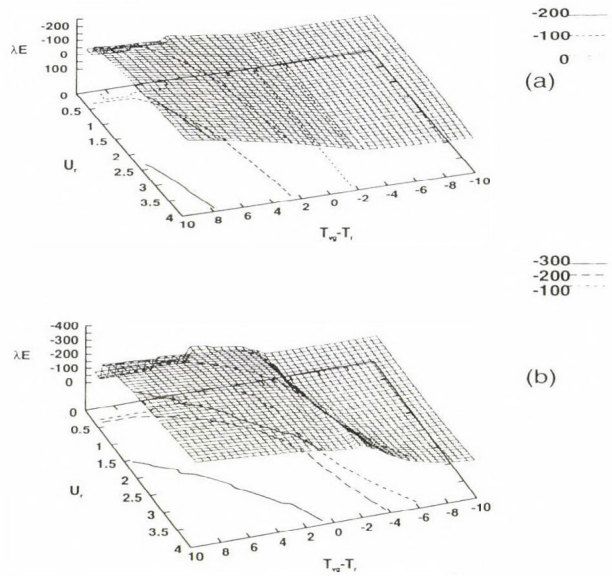

Fig. 9. The latent heat flux versus the surface/air temperature difference $T_{vg} - T_r$ and the wind velocity for (*a*) $RH = 90$ per cent ("wet" case) and (*b*) $RH = 30$ per cent ("dry" case).

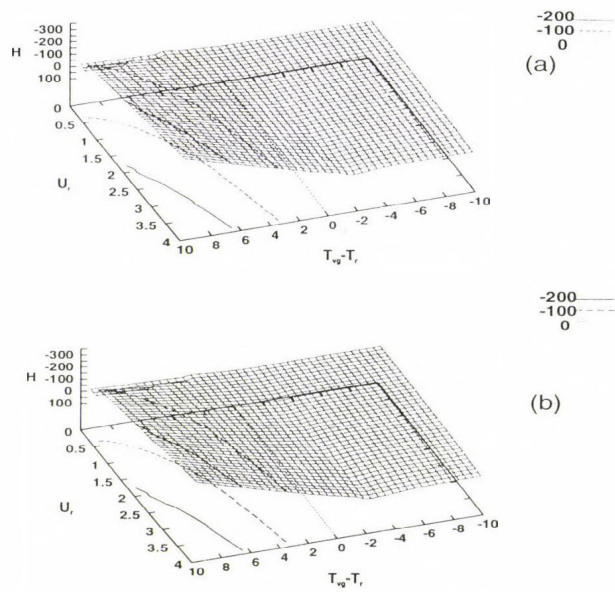

Fig. 10. The sensible heat flux versus the surface/air temperature difference $T_{vg} - T_r$ and the wind velocity for (*a*) $RH = 90$ per cent ("wet" case) and (*b*) $RH = 30$ per cent ("dry" case).

- r_a^v and u_*

In strong unstable conditions (great positive surface/air temperature difference and strong wind), $r_a(T_{vg}-T_r,U_r)$, is about 40 s m^{-1}, so for example r_a^v(9.5°C, 3.9 m s^{-1})=37 s m^{-1}. In strong stable conditions (great negative surface/air temperature difference and small wind) r_a^v values are about 5000 s m^{-1}. In the left (great positive surface/air temperature difference and small wind) and right (great negative surface/air temperature difference and strong wind) corners of the field r_a^v is about the same of 360 s m^{-1}.

The greatest u_* values are between 0.3 and 0.4 in the strong unstable stratification. The $u_*(T_{vg}-T_r,U_r)$ field decreases towards decreasing surface/air temperature difference and wind. For small winds —independently from the temperature difference forcing— the u_* values are extremely small. In the simulations the lower limit of u_* values is taken as 0.02 m s^{-1}. Two facts can also be observed: the relative sharp boundary between the unstable and stable stratifications and that u_* values decrease with decreasing wind in both stratifications. Since u_* (–10°C, 3.9 m s^{-1})=0.09 m s^{-1} this decrease is obviously greater in the unstable stratification than in the stable one.

- $\lambda \cdot E$ and H

According to our convention, $\lambda \cdot E$ is negative in unstable and positive in stable stratification. The $\lambda \cdot E$ field is very similar to u_* field. Its characteristics agree with u_* field characteristics: in strong unstable stratification the $\lambda \cdot E$ values are between –300 and –400 W m^{-2} and decrease towards decreasing surface/air temperature difference and wind. In the left corner of the field (free convection zone) $\lambda \cdot E$ values are about –100 W m^{-2}. In spite of this the $\lambda \cdot E$ values are about –50 W m^{-2} in the right corner of the field (stable stratification with moderate wind), that is they are about two times smaller than in the state of free convection. In the strong stable stratification (great negative surface/air temperature difference and extremely weak wind) $\lambda \cdot E$ is very close to zero but still positive.

The H field is also similar to the field of u_* and $\lambda \cdot E$ but there is a basic deviation: the minimum of H is not in the region of small winds and great negative surface/air temperature differences (H (–10°C, 0.1 m s^{-1})=2 W m^{-2}) but in the region of stable stratification with moderate winds (H (–10°C, 3.9 m s^{-1})= 32 W m^{-2}). In the free convection zone H is not great (H (9.5°C, 0.1 m s^{-1})= –32 W m^{-2}). In spite of this in strong unstable conditions H can reach –300 W m^{-2}.

4. Conclusions

The surface aerodynamic transfer parameterization method SAPA is described, tested and analyzed in terms of its numerical and physical features. The physics of the scheme is based on the M-O similarity theory. It differs from similar M-O based schemes in the application of the numerical procedure for solving the implicitly defined equation system (Eqs. from (1) to (24)). The fixed-point method (Eq. (27)) is applied. We demonstrated that—though an iterative procedure is used—the method seems to be reliable not only in the common but also in the extreme cases. We have also proved the performance of the scheme on the Cabauw data set. According to these results, the scheme seems to be quite reliable. Analyzing the dependence of the scheme upon the main forcing factors (the surface-air temperature difference and the wind velocity), we observed some new and interesting features. Among others:

- In general the number of iteration steps N_i is greater in stable stratification than in unstable one. N_i is determined by the wind velocity in the greatest extent.
- The initial values of $\chi = \frac{1}{L}$ determine the rate of the convergence. So N_i has a minimum in stable stratification for small winds at $\chi \approx 2$ m^{-1}.
- The fields of u_*, $\lambda \cdot E$ and H are quite similar. The similarity is more pronounced in "dry" than in "wet" case.

In the simulations, the surface resistance—a very important factor—is used as constant. Further we assumed that the surface resistance and the surface/air temperature difference are independent from each other. Presently, these assumptions are used because of the simplicity. By modeling both the surface resistance and its relation to the surface/air temperature difference, it would be possible to get a somewhat more sophisticated scheme with necessary key ingredients to do near surface climate diagnostics. This is a task for the future.

Acknowledgements—This study is financially supported by both the Österreichische Akademie der Wissenschaften within the National Austrian Committee for the IGBP and the Hungarian Ministry for Culture and Education via OTKA Foundation, project number T-029358. The authors wish to thank to *Professor Michael Hantel* for his motivation, ideas and helpful discussions. Further we especially appreciate *Mr. Zoltán Barcza*'s help transforming the text from Latex to Winword.

Appendix

The fixed-point method application

Let χ_0 be an arbitrary real number and let us define the following iteration procedure:

$$\chi_{n+1} = F(\chi_n). \tag{A.1}$$

If the iteration (A.1) is convergent, i.e., there exists $\lim_{n\to\infty} \chi_n = \chi^*$ then by (A.1)

$$\lim_{n\to\infty} \chi_n = \lim_{n\to\infty} F(\chi_n). \tag{A.2}$$

Since $F(\chi)$ is continuous function, $\lim_{n\to\infty} F(\chi_n) = F(\lim_{n\to\infty} \chi_n) = F(\chi^*)$. So Eq. (A.2) can be rewritten as

$$\chi^* = F(\chi^*). \tag{A.3}$$

Lastly according to Eq. (A.3), χ^* is the solution of the equation $\chi = F(\chi)$.

References

Ács, F. and *Hantel, M.*, 1998: The Land-Surface Flux Model PROGSURF. *Global Planet Change, 19*, 19-34.

Ács, F., Hantel, M. and *Unegg, J.W.*, 2000: Climate diagnostics with The Budapest-Vienna Land-Surface Model SURFMOD. *Austrian Contributions to the Global Change Program.* Austrian Academy of Sciences, Vol. 3, 116 pp.

Beljaars, A.C.M. and *Bosveld, F.C.*, 1997: Cabauw data for the validation of land surface parameterization schemes. *J. Climate 10*, 1172-1194.

Berkowicz, R. and *Prahm, L.P.*, 1982: Evaluation of the profile method for estimation of surface fluxes of momentum and heat. *Atmos. Environ. 16*, 2809-2819.

Businger, J., Wyngaard, J., Izumi, Y. and *Bradley, E.*, 1971: Flux-profile relationships in the atmospheric surface layer. *J. Atmos. Sci. 28*, 181-189.

Byun, D., 1990: On the analytical solutions of flux-profile relationships for the atmospheric surface layer. *J. Appl. Meteorol. 29*, 652-657

Deardorff, J.W., 1972: Numerical investigation of neutral and unstable planetary boundary layers. *J. Atmos. Sci. 29*, 91-115.

de Bruin, H.A.R., Ronda, R.J. and *Van De Wiel, B.J.H.*, 2000: Approximate solutions for the Obukhov length and the surface fluxes in terms of bulk Richardson Numbers. *Boundary-Layer Meteorol. 95*, 145-157.

Holtslag, A.A.M. and *van Ulden, A.P.*, 1983: A simple scheme for daytime estimates of the surface fluxes from routine weather data. *J. Climate Appl. Meteorol. 22*, 517-529.

Holtslag, A.A.M. and *de Bruin, H.A.R.*, 1988: Applied modelling of the nighttime surface energy balance over land. *J. Appl. Meteorol. 27*, 689-704.

Kovács, M. and *Ács, F.*, 2000: A Surface Aerodynamic Transfer Parameterization Method: Numerical Studies For Different Stability Regimes. CD rom of the EGS 25th General Assembly, Geophysical Research Abstracts, ISSN: 1029-7006, 2, Nice, 24-29 April.

Lee, H.N., 1997: Improvement of surface flux calculations in the atmospheric surface layer. *J. Appl. Meteorol 36*, 1416-1423

Louis, J.-F., 1979: A parametric model of vertical eddy fluxes in the atmosphere. *Bound.-Layer Meteorol. 17*, 187-202

Manju, K. and *Sharma, O.P.*, 1987: Estimation of turbulence parameters for application in air pollution modelling. *Mausam 38*, 303-308.

Mohan, M. and *Siddiqui, T.A.*, 1998: Applied modeling of surface fluxes under different stability regimes. *J. Appl. Meteorol. 37*, 1055-1067.

Noilhan, J. and *Planton, S.*, 1989: A simple parameterization of land surface processes for meteorological models. *Mon. Wea. Rev. 117*, 536-549.

Schayes, G., 1982: Direct determination of diffusivity profiles from synoptic reports. *J. Atm. Sci. 27*, 1122-1137.

Wetzel, P.J. and *Chang, Y. T.*, 1988: Evapotranspiration from nonuniform durfaces: A first approach for short term numerical weather prediction. *Mon. Wea. Rev. 116*, 600-621.

BOOK REVIEW

Ruddiman, W. F., 2001: **Earth's Climate—Past and Future.** W. H. Freeman and Company, New York. 465 pages, over four hundred four color illustrations, extended glossary and index.

The author is a geologist, professor of the Department of Environmental Sciences at the University of Virginia, USA. This fact largely determines the key value of the book for meteorologists and other scientists, trained in climatology of relatively short time scales. The issue depicts interactions within Earth's climate system at all scales, indexes of climate change, evidence of the past climate changes, and projections of possible future changes.

The author recommends the volume "To five colleagues who headed the effort to make the study of Earth's climate a science: *John Imbrie, John Kutzbach, Wally Broecker, Nick Shackleton* and *Murray Mitchell.*" These names, as the most affecting banner, demonstrate the widest geophysical scope that promises special value among the numerous volumes, already written about the topic.

The book moves step-by-step through logically developed summaries of the major lessons learned from 550 million years of climate changes, including the impact on and by humans. The five parts of the book are: "Framework of Climate Science"; "Tectonic-Scale Climate Change"; "Orbital-Scale Tectonic-Scale Climate Change"; "Deglacial and Millennial Climate Change"; and "Historical and Future Climate Change". After a balanced and fairly informative introduction to the climate system, this classification is motivated by the peculiarities of climate represent separation climate. The second part represents the recent 10% of the Eath's age, an interval during which mammals evolved from primitive to more distinctive forms. Part Three looks at the last 3 million years, a time span when our species was rapidly evolving towards its present form. Part Four explores changes over the last 50,000 years, an interval during which humans initially lived a primitive hunting-and-gathering life. Then developed and practiced agriculture and created the first recorded human civilizations. The final Part describes how changes in Earth's climate may have influenced the biological and cultural development of the human species. Its last chapter also makes predictions about "Climate Change in the Next 100 to 1000 years".

The features and recurring themes, that link together sections of the text, include glaciations, intensity of monsoons, flow of deep water in the ocean, the

role of carbon as it moves through the Earth system, and other factors that contribute to icehouse (!) or greenhouse worlds.

Summarizing, the reader meets an excellent introductory volume into the climate science, with clear qualitative explanation of the processes at all scales, driven by any branch of natural sciences. The additional Glossary, itself, counts eight A4 pages, where many definitions apply specifically to their use in climatic studies. The text is accompanied by a large number of colored figures that are clear and well explained in their captions.

J. Mika

ATMOSPHERIC ENVIRONMENT

an international journal

To promote the distribution of Atmospheric Environment *Időjárás* publishes regularly the contents of this important journal. For further information the interested reader is asked to contact *Prof. P. Brimblecombe*, School for Environmental Sciences, University of East Anglia, Norwich NR4 7TJ, U.K.; E-mail: atmos_env@uea.ac.uk

Volume 35 Number 7 2001

Short communication

S.G. Yeatman, L.J. Spokes, P.F. Dennis and *T.D. Jickells:* Can the study of nitrogen isotopic composition in size-segregated aerosol nitrate and ammonium be used to investigate atmospheric processing mechanisms? 1337-1345.

Volume 35 Number 8 2001

J. Kuebler, H. van den Bergh and *A.G. Russel:* Long-term trends of primary and secondary pollutant concentrations in Switzerland and their response to emission controls and economic changes, 1351-1364.

C.A. Pio, C.A. Alves and *A.C. Duarte:* Identification, abundance and origing of atmospheric organic particulate matter in a Portuguese rural area, 1365-1376.

A. Ezcurra, I. Ortiz de Zárate, P.V. Dhin and *J.P. Lacaux:* Cereal waste burning pollution observed in the town of Vitoria (northern Spain), 1377-1386.

A. Charron, P. Coddeville, S. Sauvage, J.-C. Galloo and *R. Guillermo*: Possible source areas and influential factors for sulphur compounds in Morvan, Fance, 1387-1394.

M. Sofiev, G. Petersen, O. Krüger, B. Schneider, M. Hongisto and *K. Jylha:* Model simulations of the atmospheric trace metals concentrations and depositions over the Baltic Sea, 1395-1410.

R.D. Edwards and *M.J. Jantunen:* Benzene exposure in Helsinki, Finland, 1411-1420.

S. Huang, R. Arimoto and *K.A. Rahn:* Sources and source variations for aerosol at Mace Head, Ireland, 1421-1438.

L. Brown, S.A. Brown, S.C. Jarvis, B. Syed, K.W.T. Goulding, V.R. Philips, R.W. Sneath and *B.F. Pain*: An inventory of nitrous oxide emissions from agriculture in the UK using the IPCC methodology: emission estimate, uncertainty and sensitivity analysis, 1439-1450.

J.R. Stedman, J.W.L. Goodwin, K. King, T.P. Murrells and *T.J. Bush:* An empirical model for predicting urban roadside nitrogen dioxide concentrations in the UK, 1451-1464.

I.K. Koponen, A. Asmi, P. Keronen, K. Puhto and *M. Kulmala:* Indoor air measurement campaign in Helsinki, Finland 1999 – the effect of outdoor air pollutinon on indoor air, 1465-1478.

C.I. Beattie, J.W.S. Longhurst and *N.K. Woodfield:* Air quality management: evolution of policy and practice in the UK as exemplified by the experience of English local government, 1479-1490.

Volume 35 Number 9 2001

R.N. Colvile, E.J. Hutchinson, J.S. Mindell and *R.F. Warren:* The transport sector as a source of air pollution, 1537-1565.

J.G. Watson, J.C. Chow and *E.M. Fujita:* Review of volatile organic compound source apportionment by chemical mass balance, 1567-1584.

C.Y.H. Chao and *T.C. Tung:* An empirical model for outdoor contaminant transmission into residential buildings and experimental verification, 1585-1596.

S. Du: A heuristic Lagrangian stochastic particle model of relative diffusion: model formulation and preliminary results, 1597-1607.

R. De Winter-Sorkina: Impact of ozone layer depletion I: ozone depletion climatology, 1609-1614.

R. De Winter-Sorkina: Impact of ozone layer depletion II: changes in photodissociation rates and tropospheric composition, 1615-1625.

Volume 35 Number 10 2001

NOTES TO CONTRIBUTORS

The purpose of *Időjárás* is to publish papers in the field of theoretical and applied meteorology. These may be reports on new results of scientific investigations, critical review articles summarizing current problems in certain subject, or shorter contributions dealing with a specific question. Authors may be of any nationality but papers are published only in English.

Papers will be subjected to constructive criticism by unidentified referees.

* * *

The manuscript should meet the following formal requirements:

Title should contain the title of the paper, the names(s) of the author(s) with indication of the name and address of employment.

The title should be followed by an *abstract* containing the aim, method and conclusions of the scientific investigation. After the abstract, the *key-words* of the content of the paper must be given.

Three copies of the manuscript, typed with double space, should be sent to the Editor-in-Chief: *P.O. Box 39, H-1675 Budapest,* Hungary.

References: The text citation should contain the name(s) of the author(s) in Italic letter or underlined and the year of publication. In case of one author: *Miller* (1989), or if the name of the author cannot be fitted into the text: *(Miller,* 1989); in the case of two authors: *Gamov* and *Cleveland* (1973); if there are more than two authors: *Smith et al.* (1990). When referring to several papers published in the same year by the same author, the year of publication should be followed by letters a,b etc. At the end of the paper the list of references should be arranged alphabetically. For an article: the name(s) of author(s) in Italics or underlined, year, title of article, name of journal, volume number (the latter two in Italics or underlined) and pages. E.g. *Nathan, K. K.,* 1986: A note on the relationship between photosynthetically active radiation and cloud amount. *Időjárás 90,* 10-13. For a book: the name(s) of author(s), year, title of the book (all in Italics or underlined with except of the year), publisher and place of publication. E.g. *Junge, C. E.,* 1963: *Air Chemistry and Radioactivity.* Academic Press, New York and London.

Figures should be prepared entirely in black India ink upon transparent paper or copied by a good quality copier. A series of figures should be attached to each copy of the manuscript. The legends of figures should be given on a separate sheet. Photographs of good quality may be provided in black and white.

Tables should be marked by Arabic numbers and provided on separate sheets together with relevant captions. In one table the column number is maximum 13 if possible. One column should not contain more than five characters.

Mathematical formulas and *symbols:* non-Latin letters and hand-written marks should be explained by making marginal notes in pencil.

The final text should be submitted both in manuscript form and on *diskette.* Use standard 3.5" or 5.25" DOS formatted diskettes for this purpose. The following word processors are supported: WordPerfect 5.1, WordPerfect for Windows 5.1, Microsoft Word 5.5, Microsoft Word 6.0. In all other cases the preferred text format is ASCII.

* * *

Authors receive 30 *reprints* free of charge. Additional reprints may be ordered at the authors' expense when sending back the proofs to the Editorial Office.

Published by the Hungarian Meteorological Service

Budapest, Hungary

INDEX: 26 361

HU ISSN 0324-6329

IDŐJÁRÁS

VOLUME 105 * 2001

BUDAPEST, HUNGARY

AUTHOR INDEX

TABLE OF CONTENTS

I. Papers

II. Book review

III. Contents of journal Atmospheric Environment, 2001

IV. SUBJECT INDEX

The asterisk denotes book reviews

T

W

X

GUIDE FOR AUTHORS OF *IDŐJÁRÁS*

The purpose of the journal is to publish papers in any field of meteorology and atmosphere related scientific areas. These may be

- research papers on new results of scientific investigations,
- critical review articles summarizing the current state of art of a certain topic,
- short contributions dealing with a particular question.

Some issues contain "News" and "Book review", therefore, such contributions are also welcome. The papers must be in American English and should be checked by a native speaker if necessary.

Authors are requested to send their manuscripts to

Editor-in Chief of IDŐJÁRÁS

P.O. Box 39, H-1675 Budapest, Hungary

in three identical printed copies including all illustrations. Papers will then be reviewed normally by two independent referees, who remain unidentified for the author(s). The Editor-in-Chief will inform the author(s) whether or not the paper is acceptable for publication, and what modifications, if any, are necessary.

Please, follow the order given below when typing manuscripts.

Title part: should consist of the title, the name(s) of the author(s), their affiliation(s) including full postal and E-mail address(es). In case of more than one author, the corresponding author must be identified.

Abstract: should contain the purpose, the applied data and methods as well as the basic conclusion(s) of the paper.

Key-words: must be included (from 5 to 10) to help to classify the topic.

Text: has to be typed in double spacing with wide margins on one side of an A4 size white paper. Use of S.I. units are expected, and the use of negative exponent is preferred to fractional sign. Mathematical formulae are expected to be as simple as possible and numbered in parentheses at the right margin.

All publications cited in the text should be presented in a *list of references*, arranged in alphabetical order. For an article: name(s) of author(s) in Italics, year, title of article, name of journal, volume, number (the latter two in Italics) and pages. E.g., *Nathan, K.K.,* 1986: A note on the relationship between photo-synthetically active radiation and cloud amount. *Időjárás 90,* 10-13. For a book: name(s) of author(s), year, title of the book (all in Italics except the year), publisher and place of publication. E.g., *Junge, C. E.,* 1963: *Air Chemistry and Radioactivity*. Academic Press, New York and London. Reference in the text should contain the name(s) of the author(s) in Italics and year of publication. E.g., in the case of one author: *Miller* (1989); in the case of two authors: *Gamov* and *Cleveland* (1973); and if there are more than two authors: *Smith et al.* (1990). If the name of the author cannot be fitted into the text: *(Miller,* 1989); etc. When referring papers published in the same year by the same author, letters a, b, c, etc. should follow the year of publication.

Tables should be marked by Arabic numbers and printed in separate sheets with their numbers and legends given below them. Avoid too lengthy or complicated tables, or tables duplicating results given in other form in the manuscript (e.g., graphs)

Figures should also be marked with Arabic numbers and printed in black and white in camera-ready form in separate sheets with their numbers and captions given below them. Good quality laser printings are preferred.

The text should be submitted both in manuscript and in electronic form, the latter on diskette or in E-mail. Use standard 3.5" MS-DOS formatted diskette or CD for this purpose. MS Word format is preferred.

Reprints: authors receive 30 reprints free of charge. Additional reprints may be ordered at the authors' expense when sending back the proofs to the Editorial Office.

More information for authors is available: antal.e@met.hu

Information on the last issues: http://omsz.met.hu/irodalom/firat_ido/ido_hu.html

Published by the Hungarian Meteorological Service

Budapest, Hungary

INDEX: 26 361

HU ISSN 0324-6329